Spectrochimica Acta Part A: Molecular and Biomolecular Spectroscopy 255 (2021) 119669

Contents lists available at ScienceDirect

Spectrochimica Acta Part A: Molecular and Biomolecular Spectroscopy

journal homepage: www.elsevier.com/locate/saa

5-Substituted isatin thiosemicarbazones as inhibitors of tyrosinase: Insights of substituent effects

Run Cheng [a,b], Wenyan Shi [b], Qingyun Yuan [b,c], Ruiren Tang [a], Yujie Wang [b], Di Yang [b], Xin Xiao [b], Jianping Zeng [b], Jingwen Chen [b,*], Yanqing Wang [d,*]

[a] College of Chemistry and Chemical Engineering, Central South University, Changsha 410000, PR China
[b] School of Chemistry and Chemical Engineering, Building Materials Research Academy, Yancheng Institute of Technology, Jianjun East Rd. 211, Yancheng 224051, PR China
[c] School of Chemistry and Chemical Engineering, Jiangsu University, Xuefu Rd. 301, Zhenjiang 212013, PR China
[d] College of Chemistry and Environmental Engineering, Institute of Environmental Toxicology and Environmental Ecology, Yancheng Teachers University, Xiwang Avenue South Rd. 2, Yancheng 224007, PR China

HIGHLIGHTS

- Seven thiosemicarbazones TSC-ISA-**R** as tyrosinase inhibitors were synthesized.
- The inhibition effects of TSC-ISA-**R** are related to the substituent modifications.
- The inhibition effects of TSC-ISA-**R** are correlated closely with affinities to tyrosinase.
- Three potential non-covalent interactions are probably involved in the inhibition.

GRAPHICAL ABSTRACT

Seven isatin thiosemicarbazone derivatives (TSC-ISA-**R**) bearing different substituents attached at C-5 of the indoline ring were evaluated as inhibitors of mushroom tyrosinase (TYR). Three potential non-covalent interactions rather than complexation including TSC-ISA-**R** binding with TYR, TYR-L-DOPA complex, and substrate L-DOPA were probably involved in the inhibition of TSC-ISA-**R** against TYR.

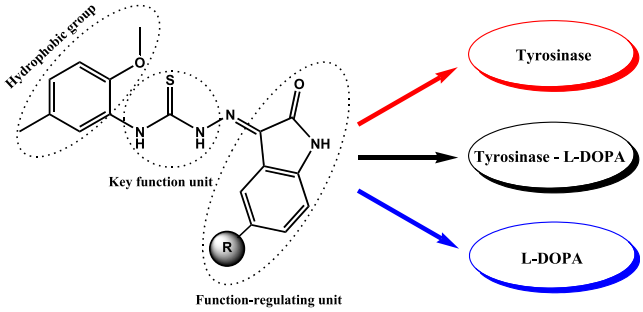

ARTICLE INFO

Article history:
Received 14 December 2020
Received in revised form 22 February 2021
Accepted 28 February 2021
Available online 9 March 2021

Keywords:
Isatin thiosemicarbazone derivatives
Tyrosinase inhibitors
Inhibition mechanism
Substituent effects

ABSTRACT

Seven isatin-thiosemicarbazone analogues bearing different substituents (**R**) attached at C-5 of the indoline ring, TSC-ISA-**R** (**R** = -H, -CH_3, -OCH_3, -OCF_3, -F, -Cl and -NO_2), were synthesized and evaluated as inhibitors of mushroom tyrosinase (TYR). The inhibitory behaviour and performance of TSC-ISA-**R** were investigated spectroscopically in relation to the substituent modifications through examining their inhibition against the diphenolase activity of TYR using *L*-DOPA as a substrate. The IC_{50} values of TSC-ISA-**R** were determined to be in the range of 81–209 μM. The kinetic analysis showed that TSC-ISA-**R** were reversible and mixed type inhibitors. Three potential non-covalent interactions rather than complexation including the binding of TSC-ISA-**R** with free TYR, TYR-*L*-DOPA complex, and with substrate *L*-DOPA were found to be involved in the inhibition. The substituent modifications affected these interactions by varying the characters of the resulting TSC-ISA-**R** in different degrees. The thiosemicarbazido moiety of each TSC-ISA-**R** contributed predominantly to the inhibition, and the isatin moiety seemed to play a regulatory role in the binding of TSC-ISA-**R** to the target molecules. The results of theoretical calculations using density functional theory method indicated a different effect of –**R** on the electron distribution in HOMO of

* Corresponding authors.
E-mail addresses: jwchen@ycit.edu.cn (J. Chen), wyqing76@126.com (Y. Wang).

https://doi.org/10.1016/j.saa.2021.119669

TSC-ISA-**R**. The LUMO-HOMO energy gap of TSC-ISA-**R** almost accords with the trend of their experimental inhibition potency.

1. Introduction

Tyrosinase (EC 1.14.18.1, abbr. TYR), also known as phenoloxidase, is a crucial dinuclear copper-containing metalloenzyme widely present in animals, plants, and microorganisms [1–6]. With the help of oxygen, the enzyme catalyzes the hydroxylation of tyrosine into *o*-diphenols (monophenolase) and the oxidation of *o*-diphenols into their *o*-quinone derivatives (diphenolase) for the production of melanin [7–9]. For mammals, such melanogenesis has been known to play an important role in multiple physiological and pathological pathways [9]. However, hyperactivity of TYR was proved to be capable of leading to overproduction of melanin accumulated in skin, which is implicated in the induction and development of a range of dermatological disorders, such as freckles, melasma, post inflammatory melanoderma, age spots, and even malignant melanoma [10–12]. In addition, the TYR-catalyzed conversion of tyrosine to dopaqone may cause neurotoxicity, which was found to correlate with neurodegenerative diseases such as Alzheimer's as well as Parkinson's and Huntington's diseases [13]. For insects, TYR activity was found to be closely associated with the physiological processes including melanin formation, wound healing, resistance to parasites and skin keratinization [14]. Furthermore, TYR is responsible for browning in plant-derived foods, which affects the shelf life of fresh-cut products and changes their sensory and gustatory properties as well as nutrition characteristics of the protein [15]. Therefore, it is quite significant to develop TYR inhibitors since these compounds can not only find potential applications in medication, insecticide, cosmetic and food industry [6,11,12,16], but also be employed to decipher the catalytic mechanism of TYR [17,18].

Over the past years, a large number of naturally occurring and synthetic compounds have been evaluated as TYR inhibitors [19–22]. In the researches, considerable efforts were concentrated on the inhibitory mechanism, structure-activity relationships as well as the molecular design and synthesis. Despite great progress, there is still a long way to go in these aspects in that few compounds have so far been put into practical applications for various reasons [12,21]. Studies revealed that there are two copper ions as the active sites and a lipophilic long-narrow gorge near the active center in the enzyme [1–6]. Generally, the synthetic TYR inhibitors were designed by a direct strategy to target the active sites of TYR by virtue of the donor atoms on inhibitor molecules for potential coordination with the copper(II) ions [18,22,23]. Another strategy is to structurally mimic the natural TYR substrates, *L*-tyrosine or/and *L*-3,4-dihydroxyphenylalanine (*L*-DOPA) [19–22]. Those containing hydrophobic groups were proven to have strong affinity to the enzyme and usually displayed high inhibitory potency due to the strong interactions between the hydrophobic groups and the residues present in the hydrophobic cavity of TYR [18,22–24].

Thiosemicarbazones (abbr. TSCs), known as chelating agents for metal ions [25], have been received considerable attention over the past decades in the field of medicinal chemistry because of their promising biological implications and remarkable pharmacological properties [26]. A number of TSC derivatives have also been evaluated as inhibitors for TYR [22,23,27,28] as well as melanogenesis [12]. In most cases, those bearing hydrophobic aryl substituents close to the thiosemicarbazido moieties exhibited more potent inhibition competency [12,18,22–24,27–38]. In general, the inhibition efficacies of these TSCs were proposed to be resulted from the enhanced interactions between their hydrophobic substituents and the hydrophobic residues in TYR cavity through van der Waals forces, as well as the ability of their N–N–S tridentate scaffold to chelate the catalytic copper ions in the enzyme. The representative instances are the aldehyde- and ketone-TSCs prepared by Jung and coauthors aiming to inhibit melanogenesis in melanoma B16 cells [29–32]. The introduction of hydrophobic substituents on the aromatic ring was found to enhance the inhibitory capacity of the resultant TSCs. Further replacement of the benzylidene hydrogen in aldehyde-TSCs or the terminal amino hydrogen (*i.e.* N^4-*H*) of aldehyde- and ketone-TSCs by hydrophobic groups can appreciably improve the inhibitory efficacy. It is evident that the hydrophobicity of the substituents introduced to TSC scaffold can remarkably influence the inhibition potency of the resulting TSCs.

Isatin (*i.e.* 1H-indole-2,3-dione) is a natural composition found in certain plants including *Calanthe discolor* (Lindl.) and *Couroupita guianensis*, and also a metabolic derivative of adrenaline hormone in humans and a component of secretion from the parotid gland of *Bufo frogs* [39]. Also, isatin and its derivatives were found to possess a wide range of pharmacological properties [40,41]. Among them, the substitution at C-5 position of indoline ring has previously been associated with increased biological activity for a range of indole-based compounds [41].

Given the biological and pharmacological properties of TSC and isatin derivatives, it is expected that the combination of both functionalities in a single entity may give rise to molecules featuring novel biological activities. Isatin features a six-membered aromatic and a five-membered anti-aromatic cyclic ring. Insertion of isatin functionality into a TSC molecule generating isatin-TSC hybrid may alter hydrophobicity of the TSC, and contribute to its steric effects through the ability of the bulky ring to occupy the binding site of molecular targets. Up to now, there have been reports on isatin-TSCs concerning the evaluation for DNA binding analysis, antimicrobial [42] and anti-viral [43] activity assay, inhibition against P-glycoprotein (P-gp) [44] and mitigation of metal corrosion [45]. However, few structures bearing isatin functionality in the aromatic moiety of TSCs were investigated as TYR inhibitor. In this study, seven isatin-TSCs with different substituents (**R**) attached at C-5 of the isatin ring, TSC-ISA-**R** (**R** = -H, $-CH_3$, $-OCH_3$, $-OCF_3$, -Cl, -F and $-NO_2$), were synthesized using 4-(2-methoxy-5-methylphenyl)thiosemicarbazide as a starting reactant. Their inhibition against the diphenolase activity of TYR was evaluated with *L*-DOPA substrate using mushroom TYR as a model system. The structural features of the inhibitors were examined using density functional theory method at B3LYP level with 6-31G (d) basis set, and the relevant parameters were obtained. To define the role of thiosemicarbazido functionality of TSC-ISA-**R** in the inhibition, the corresponding parent 5-substituted isatin compounds were examined in parallel. Moreover, the effects of substituent modifications of TSC-ISA-**R** on their affinity to TYR, and further on their inhibition against TYR activity were tentatively studied. To our knowledge, this is the first time to report the inhibitory effects of such compounds on TYR. We hope that this study could offer useful information for the future molecular design of TYR inhibitors.

2. Experimental

2.1. Chemistry and apparatus

All reagents used in this work are of analytical grade, and are commercially available. All solvents used were purchased from

Sino-pharm Chemical Reagent Co., Ltd., and purified by the reported procedures [46] prior to use. Mushroom tyrosinase and *L*-DOPA were purchased from Sigma-Aldrich. The reagents for synthesis of the inhibitors, 2-isothiocyanato-1-methoxy-4-methylbenzene, hydrazine hydrate (80%), indoline-2,3-dione, 5-methylindoline-2,3-dione, 5-methoxyindoline-2,3-dione, 5-fluoroindoline-2,3-dione, 5-chloroindoline-2,3-dione, 5-nitroindoline-2,3-dione and 5-(trifluoromethoxy)indoline-2,3-dione, were purchased from Acros Organics. During the synthesis of TSC-ISA-**R** derivatives, the reaction progress was monitored by thin layer chromatography (TLC) analysis (silica gel 60 F254, Qingdao Ocean Chemicals, China). All aqueous solutions were prepared using doubly-distilled water.

The high resolution electrospray ionization mass spectra were obtained on an Agilent 1290–6545 electron spray mass spectrometer, in ESI + mode. The ^{1}H NMR and ^{13}C NMR spectra were recorded on a Bruker DRX-400 spectrometer at 293 K in deuterated reagent DMSO d_6 (Sigma-Aldrich) as solvent. Chemical shifts (δ) were expressed in parts per million (ppm), and multiplicity was reported as s (singlet), d (doublet), t (triplet), m (multiplet), dd (double doublet), and coupling constants (J) in hertz. Elemental analyses for C, H and N were performed on a Vario EL Cube elemental analyzer (Elementar, Germany). Infrared spectra were recorded on a NEXUS 670 spectrometer (Thermo, USA) as KBr disks in the range of 4000–500 cm^{-1}. The experiments for the activity inhibition of mushroom TYR were performed on a spectrofluorometer (JASCO, FP6500, Japan) and Ultraviolet–visible (UV–vis) spectrophotometer (Shimadzu, UV2450, Japan).

2.1.1. Synthesis of 4-(2-methoxy-5-methylphenyl)thiosemicarbazide

4-(2-Methoxy-5-methylphenyl)thiosemicarbazide was synthesized referring the literature method described previously [47]. Hydrazine monohydrate (1.30 g, 22.30 mmol) was dropped slowly into a solution of 2-isothiocyanato-1-methoxy-4-methylbenzene (2.00 g, 11.16 mmol) in dichloromethane (20 mL) at room temperature under stirring. After completion of the reaction, the resultant precipitant was filtered off, washed with dichloromethane (3 × 15 mL) and diethyl ether (2 × 15 mL). The crude product was recrystallized using n-hexane (20 mL) and dried in desiccator under vacuum at room temperature. Additional amount of the title compound was recovered from the filtrate after cooling at 0 °C (water–ice bath). The obtained thiosemicarbazide was sufficiently pure based on ^{1}H NMR results, and used in the next step without further purification.

*2.1.2. General procedure for the synthesis of TSC-ISA-**R***

The title isatin-TSC derivatives were prepared referring the method previously described [48]. Briefly, equimolar quantity of 4-(2-methoxy-5-methylphenyl)thiosemicarbazide obtained above and different 5-substituted indoline-2,3-dione was combined in ethanol (20 mL) with addition of a few drops of acetic acid to initiate the reaction. The mixture was refluxed under continuous stirring, and the reaction was monitored by TLC with ethyl acetate/petroleum ether = 1/1 (v/v) as developing solvent. After completion of the reaction, the mixture was cooled to room temperature, and the resulting solid was collected using centrifugation separation, washed with water (2 × 15 mL) and diethyl ether (2 × 15 mL). The pure products were obtained by crystallization from ethanol or toluene (20 mL).

*2.1.2.1. (E)-4-(2-methoxy-5-methylphenyl)-1-(2-oxoindolin-3-ylidene)thiosemicarbazide (**TSC-ISA-H**).* Yield, 52.9%, yellow solid. Obtained from 4-(2-methoxy-5-methylphenyl)thiosemicarbazide and indoline-2,3-dione (*i.e.* isatin). FT-IR (KBr, cm^{-1}): 1619.34 (C═N), 1132.80 (C═S) (Fig. S1); Elemental analysis, found (calcd.) (%): C, 60.10 (59.98); H, 4.65 (4.74); N, 16.43 (16.46); ESI-MS found for $[C_{17}H_{16}N_4O_2S + H]^+$ (*m*/*z*): 341.1069 (calcd. 340.10) (Fig. S2); ^{1}H NMR (DMSO d_6) δ: 12.79 (s, 1H), 11.27 (s, 1H), 10.42 (s, 1H), 7.76–7.63 (m, 2H), 7.39 (td, *J* = 7.7, 1.2 Hz, 1H), 7.19–6.86 (m, 4H), 3.83 (s, 3H), 2.31 (d, *J* = 22.0 Hz, 3H) (Fig. S3). ^{13}C NMR (DMSO d_6) δ: 176.27, 163.17, 151.10, 143.02, 132.68, 131.95, 129.39, 128.03, 127.16, 126.74, 122.96, 121.47, 120.27, 112.04, 111.61, 56.36, 20.71 (Fig. S4).

*2.1.2.2. (E)-4-(2-methoxy-5-methylphenyl)-1-(5-methyl-2-oxoindolin-3-ylidene)thiosemicarbazide (**TSC-ISA-CH$_3$**).* Yield, 72.1%, pomegranate solid. Obtained from 4-(2-methoxy-5-methylphenyl)thiosemicarbazide and 5-methylindoline-2,3-dione. FT-IR (KBr, cm^{-1}): 1629.27 (C═N), 1133.83 (C═S) (Fig. S1); Elemental analysis, found (calcd.) (%): C, 61.01 (61.00); H, 4.92 (5.12); N, 15.86 (15.81); ESI-MS found for $[C_{18}H_{18}N_4O_2S + H]^+$ (*m*/*z*): 355.1226 (calcd. 354.12) (Fig. S2); ^{1}H NMR (DMSO d_6) δ: 12.76 (s, 1H), 11.16 (s, 1H), 10.41 (s, 1H), 7.61 (s, 1H), 7.52 (s, 1H), 7.19 (dd, *J* = 7.9, 0.9 Hz, 1H), 7.10 (dd, *J* = 8.4, 1.7 Hz, 1H), 7.03 (d, *J* = 8.4 Hz, 1H), 6.84 (d, *J* = 7.9 Hz, 1H), 3.83 (s, 3H), 2.30 (d, *J* = 13.4 Hz, 6H) (Fig. S3). ^{13}C NMR (DMSO d_6) δ: 176.55, 163.24, 151.40, 140.79, 132.76, 132.36, 131.94, 129.39, 128.20, 127.30, 121.87, 120.32, 112.10, 111.38, 56.33, 21.11, 20.68 (Fig. S4).

*2.1.2.3. (E)-1-(5-methoxy-2-oxoindolin-3-ylidene)-4-(2-methoxy-5-methylphenyl)thiosemicarbazide (**TSC-ISA-OCH$_3$**).* Yield, 73.1%, pale red solid. Obtained from 4-(2-methoxy-5-methylphenyl)thiosemicarbazide and 5-methoxyindoline-2,3-dione. FT-IR (KBr, cm^{-1}): 1653.10 (C═N), 1146.81 (C═S) (Fig. S1); Elemental analysis, found (calcd.) (%): C, 58.13 (58.36); H, 4.64 (3.90); N, 14.75 (15.12); ESI-MS found for $[C_{18}H_{18}N_4O_3S + H]^+$ (*m*/*z*): 371.1172 (calcd. 370.11) (Fig. S2); ^{1}H NMR (DMSO d_6) δ: 12.75 (s, 1H), 11.07 (s, 1H), 10.43 (s, 1H), 7.52 (s, 1H), 7.32 (d, *J* = 2.3 Hz, 1H), 7.11 (dd, *J* = 8.4, 1.7 Hz, 1H), 7.03 (d, *J* = 8.4 Hz, 1H), 6.96 (dd, *J* = 8.5, 2.6 Hz, 1H), 6.87 (d, *J* = 8.5 Hz, 1H), 3.79 (d, *J* = 15.1 Hz, 6H), 2.28 (s, 3H) (Fig. S3). ^{13}C NMR (DMSO d_6) δ: 176.89, 163.27, 155.79, 151.79, 136.69, 132.84, 129.45, 128.49, 127.92, 127.15, 121.13, 118.08, 112.39, 112.20, 106.57, 56.27, 56.03, 20.62 (Fig. S4).

*2.1.2.4. (E)-4-(2-methoxy-5-methylphenyl)-1-(2-oxo-5-(trifluoromethoxy)indolin-3-ylidene)thiosemicarbazide (**TSC-ISA-OCF$_3$**).*

Yield, 79.0%, pale red solid. Obtained from 4-(2-methoxy-5-methylphenyl)thiosemicarbazide and 5-(trifluoromethoxy)indoline-2,3-dione. FT-IR (KBr, cm^{-1}): 1627.38 (C═O), 1145.03 (C═S) (Fig. S1); Elemental analysis, found (calcd.) (%): C, 50.94 (50.94); H, 3.46 (3.56); N, 13.12 (13.20); ESI-MS found for $[C_{18}H_{15}N_4O_3S + H]^+$ (*m*/*z*): 425.0890 (calcd. 424.08) (Fig. S2); ^{1}H NMR (DMSO d_6) δ: 12.61 (s, 1H), 11.41 (s, 1H), 10.54 (s, 1H), 7.74 (s, 1H), 7.38 (s, 2H), 7.13 (d, *J* = 7.3 Hz, 1H), 7.04 (d, *J* = 8.4 Hz, 2H), 3.80 (s, 3H), 2.28 (s, 3H) (Fig. S3). ^{13}C NMR (DMSO d_6) δ: 177.27, 163.22, 152.21, 144.05, 141.81, 131.51, 129.47, 128.84, 128.69, 127.02, 124.62, 121.93, 114.62, 112.67, 112.29, 56.17, 20.55 (Fig. S4).

*2.1.2.5. (E)-1-(5-fluoro-2-oxoindolin-3-ylidene)-4-(2-methoxy-5-methylphenyl)thiosemicarbazide (**TSC-ISA-F**).* Obtained from 4-(2-methoxy-5-methylphenyl)thiosemicarbazide and 5-floroindoline-2,3-dione. Yield, 84.1%, bright yellow solid. FT-IR (KBr, cm^{-1}): 1633.58 (C═N), 1137.59 (C═S) (Fig. S1); Elemental analysis, found (calcd.) (%): C, 57.06 (56.97); H, 4.31 (4.22); N, 15.32 (15.63); ESI-MS found for $[C_{17}H_{15}FN_4O_2S + H]^+$ (*m*/*z*): 359.0918 (calcd. 358.09) (Fig. S2); ^{1}H NMR (DMSO d_6) δ: 12.68 (s, 1H), 11.27 (s, 1H), 10.46 (s, 1H), 7.55 (dd, *J* = 8.1, 2.6 Hz, 1H), 7.48 (d, *J* = 1.6 Hz, 1H), 7.22 (ddd, *J* = 9.5, 8.7, 2.7 Hz, 1H), 7.12 (dd, *J* = 8.4, 1.7 Hz, 1H), 7.03 (d, *J* = 8.4 Hz, 1H), 6.95 (dd, *J* = 8.6, 4.2 Hz, 1H), 3.81 (s, 3H), 2.28 (s, 3H) (Fig. S3). ^{13}C NMR (DMSO d_6) δ: 176.88, 163.25, 151.78,

139.23, 132.02, 129.42, 128.55, 127.96, 127.01, 121.82, 121.73, 118.22, 117.97, 112.18, 108.61, 56.25, 20.61 (Fig. S4).

*2.1.2.6. (E)-1-(5-chloro-2-oxoindolin-3-ylidene)-4-(2-methoxy-5-methylphenyl)thiosemicarbazide (**TSC-ISA-Cl**).* Yield, 88.0%, pale red solid. Obtained from 4-(2-methoxy-5-methylphenyl)thiosemi carbazide and 5-chloroindoline-2,3-dione. FT-IR (KBr, cm^{-1}): 1622.78 (C═N), 1142.71 (C═S) (Fig. S1); Elemental analysis, found (calcd.) (%): C, 54.49 (54.47); H, 4.13 (4.03); N, 14.70 (14.95); ESI-MS found for $[C_{17}H_{15}ClN_4O_2S + H]^+$ (*m*/*z*): 375.0678 (calcd. 374.06) (Fig. S2); ^{1}H NMR (DMSO d_6) δ: 12.59 (s, 1H), 11.35 (s, 1H), 10.52 (s, 1H), 7.80 (d, *J* = 2.0 Hz, 1H), 7.58–7.27 (m, 2H), 7.06 (ddd, *J* = 36.2, 18.1, 5.0 Hz, 3H), 3.80 (s, 3H), 2.28 (s, 3H) (Fig. S3). ^{13}C NMR (DMSO d_6) *δ*: 177.21, 162.92, 152.13, 141.59, 131.35, 131.03, 129.43, 128.76, 128.60, 127.03, 122.32, 121.22, 113.05, 112.26, 56.20, 20.57 (Fig. S4).

*2.1.2.7. (E)-4-(2-methoxy-5-methylphenyl)-1-(5-nitro-2-oxoindolin-3-ylidene)thiosemicarbazide (**TSC-ISA-NO$_2$**).* Yield, 91.5%, pale red solid. Obtained from 4-(2-methoxy-5-methylphenyl)thiosemicar bazide and 5-nitroindoline-2,3-dione. FT-IR (KBr, cm^{-1}): 1625.32 (C═N), 1109.19 (C═S) (Fig. S1); Elemental analysis, found (calcd.) (%): C, 53.49 (52.98); H, 3.94 (3.92); N, 17.65 (18.17); ESI-MS found for $[C_{17}H_{15}N_5O_4S + H]^+$ (*m*/*z*): 386.0915 (calcd. 385.08) (Fig. S2); ^{1}H NMR (DMSO d_6) δ: 12.50 (s, 1H), 11.85 (s, 1H), 10.74 (s, 1H), 8.65 (d, *J* = 2.0 Hz, 1H), 8.29 (dd, *J* = 8.7, 2.4 Hz, 1H), 7.30 (d, *J* = 1.9 Hz, 1H), 7.14 (d, *J* = 8.7 Hz, 2H), 7.04 (d, *J* = 8.4 Hz, 1H), 3.80 (s, 3H), 2.29 (s, 3H) (Fig. S3). ^{13}C NMR (DMSO d_6) *δ*: 177.41, 163.45, 152.40, 147.97, 143.23, 130.53, 129.47, 128.98, 127.46, 127.02, 121.45, 116.96, 112.32, 111.70, 56.15, 20.54 (Fig. S4).

2.2. Assay of inhibition effects of TSC-ISA-**R** on mushroom TYR

The assay for the effects of TSC-ISA-**R** on TYR was conducted in terms of inhibiting the diphenolase activity of mushroom TYR with *L*-DOPA as a substrate, referring the procedures reported previously [49]. In the assay, each TSC-ISA-**R** and the parent 5-substituted indoline-2,3-dione were firstly dissolved in DMSO to give the corresponding stock solution. Na_2HPO_4-NaH_2PO_4 buffer solution (PBS, 50 mM, pH 6.8) was used to dilute TYR, *L*-DOPA and the DMSO stock solution of the inhibitors. Briefly, 100 μL TSC-ISA-**R** solution in different concentrations was mixed with 2800 μL *L*-DOPA (0.5 mM) in the PBS, and then a portion of 100 μL TYR solution (1000 U/mL) was added to the mixture, diluted using the PBS to desired volume and then fully mixed. The residual activity of TYR was immediately monitored by measuring the changes in absorbance of the solution at 475 nm (ε = 3.7 × 10^3 M^{-1} cm^{-1}) for *L*-dopaquinone production for 800 s at 30 °C on UV-2450 spectrophotometer equipped with a temperature control unit, using a 1.0 cm quartz cell. The blank solution included the same reagents as the test samples except for the substrate *L*-DOPA. Dose–dependent curves were obtained by performing assays in the presence of the increasing concentrations of each inhibitor. The measurements were conducted for each concentration of an inhibitor in triplicate, and the average was taken as the final result. The inhibitory efficacy of TSC-ISA-**R** was expressed as the inhibitor concentration leading to 50% loss of enzyme activity (IC_{50}) determined by interpolation of the dose-response curves. The inhibition percentage was calculated by the following equation [36]:

$$\text{Inhibition rate}(\%) = [(A_b - A_{b0}) - (A_a - A_{a0})]/(A_b - A_{b0}) \times 100\%$$

where A_a and A_b are the absorbance of the mixed solution in the presence and absence of inhibitor, respectively, and A_{a0} and A_{b0} represent the absorbance of the corresponding reagent blank solution. Kojic acid, a well-known and the most intensively studied TYR inhibitor, was selected as a positive reference.

It should be noted that the stock solution of each TSC-ISA-**R** was prepared using DMSO since TSC-ISA-**R** are poorly soluble in PBS. As declared before, organic solvents can inhibit enzymes if their concentration is higher than 3% (v/v) [50]. In the inhibition studies, the final concentration of DMSO in the reaction solutions was adjusted to not exceed 3%. Optimal ionic strength and pH for the TYR activity assay were maintained by the PBS. Considering the inhibitory effect of the solvent, the corresponding blank solutions were prepared and the relative results were recorded. Moreover, the concentration range of each inhibitor used in the measurements was controlled to avoid precipitation since the inhibitors have different solubility in the medium.

2.3. Inhibition kinetics and inhibitory type of TSC-ISA-**R** on mushroom TYR

The inhibition kinetic studies on inhibitory effects of TSC-ISA-**R** on the diphenolase activity of TYR were conducted on a UV2450 spectrophotometer by examining the *L*-dopaquinone production [24] in the presence of different concentrations of each TSC-ISA-**R**. Assays for the inhibition type were carried out by maintaining the concentration of TYR (33.3 U/mL) and varying the concentration of *L*-DOPA (0.1, 0.5, 1.0, and 1.5 mM) in the presence of different concentrations of each TSC-ISA-**R** in PBS containing 3% DMSO. The inhibition type of TSC-ISA-**R** was determined by Lineweaver-Burk plot based on the results of the inhibitory effects of each inhibitor on the diphenolase activity of TYR according to Eq. (1). The inhibitory constants (K_I) for competitive inhibition were determined by the secondary plots of the apparent Michaelis constant K_M from the Lineweaver-Burk plot versus the concentration of the inhibitor. The inhibition constants (K_{IS}) for uncompetitive and mixed-type inhibition were determined by the secondary plots of $1/V_{max}$ as the function of the inhibitor concentration [24].

$$\frac{1}{V} = \frac{K_M}{V_{max}}\left(1 + \frac{[I]}{K_I}\right)\frac{1}{[S]} \quad \frac{1}{V_{max}}\left(1 + \frac{[I]}{K_{IS}}\right) \tag{1}$$

where V and V_{max} are the reaction velocity and the maximal reaction velocity, respectively; K_M is the Michaelis constant; [I] and [S] are the concentration of inhibitor and substrate, respectively; K_I and K_{IS} are the inhibition constants for the binding of an inhibitor with the free enzyme and with the enzyme-substrate complex, respectively.

2.4. Inhibition mechanism of TSC-ISA-**R** on mushroom TYR

The inhibition mechanism of TSC-ISA-**R** on TYR was studied by examining the interactions between TSC-ISA-**R** and TYR, as well as the binding of TSC-ISA-**R** with the substrate. The former was performed by means of ESI-MS, steady-state and synchronous fluorescence and FT-IR, and the latter by ESI-MS.

A certain TSC-ISA-**R** dissolved in DMSO was added to mushroom TYR in the PBS, incubated for 30 min, and then subjected to ESI-MS analysis. The possible chelation of TSC-ISA-**R** to copper ions at the active site of TYR was ascertained by detecting the formation of TSC-ISA-**R**-Cu(II) complexes.

The fluorescence titration experiments were performed referring the previous method [34] on a FP6500 spectrofluorometer. A 3.0 mL TYR (83.3 U/mL) in PBS was titrated continuously with increasing concentrations of a TSC-ISA-**R** (0 to 46.48 μmol L^{-1}) dissolved in DMSO at 30 °C. The excitation wavelength was set at 280 nm and the emission spectra were collected from 290 to 450 nm with excitation and emission slits kept at 3 nm. The fluo-

rescence quenching constant (K_{sv}) and quenching rate constant (K_q) were calculated by Stern-Volmer equation (2) [51].

$$F_0/F = 1 + K_{sv}[Q] = 1 + K_q\tau_0[Q] \quad (2)$$

where F and F_0 represent the fluorescence intensities of a protein in the presence and absence of a quencher respectively; [Q] is the quencher concentration; K_{sv} is the Stern–Volmer quenching constant, and K_q is the rate constant of bimolecular quenching process; τ_0 is the average fluorescence lifetime of the fluorophores of fluorescent molecules in the absence of quencher, and the τ_0 value of biological macromolecules is usually taken as about 10^{-8} s [51].

For a static quenching interaction, it is assumed that there are similar and independent sites in a TYR molecule, the apparent binding constant (K_a) and the number of binding sites (n) between an inhibitor and a TYR molecule were calculated by the Eq. (3) [52].

$$\lg[(F_0 - F)/F] = n\lg[I] + \lg K_a \quad (3)$$

The synchronous fluorescence spectra were obtained at 30 °C by setting the intervals between excitation and emission wavelength at 15 nm and 60 nm respectively [37]. Successive aliquots of a certain TSC-ISA-**R** stock solution were added to a 3.0 mL of TYR solution (83.3 U/mL) using a microliter syringe. The final inhibitor concentrations were the same as those employed in the steady-state fluorescence titrations.

In order to further gain insight into the effects of the inhibitors on conformational change of mushroom TYR, FT-IR measurements were carried out referring the reported procedures [53] on a Nicolet 670 FT-IR spectrometer equipped with a germanium attenuated total reflection (ATR). Prior to measurements, the mushroom TYR was dissolved in the phosphate buffer, and each TSC-ISA-**R** was dissolved in DMSO. Aliquots of a certain TSC-ISA-**R** solution was added to the enzyme solution and mixed fully, giving rise to a mixture containing 500 U/mL of TYR and 0.5 mM of TSC-ISA-**R**. The FT-IR spectra of each mixed solution were recorded in the range of 1800–1400 cm^{-1} at room temperature. The spectrum of the blank solution containing each TSC-ISA-**R** in the same concentration in the buffer was subtracted. The characteristic absorption of the amide I band was used to analyze the structure changes of TYR resulted by the TSC-ISA-**R** binding.

The binding of TSC-ISA-**R** with *L*-DOPA was investigated by detecting whether TSC-ISA-**R**-*L*-DOPA complexes were formed under the same conditions as those in enzyme activity inhibition using ESI-MS.

All experiments were repeated at least three times and average results were taken.

2.5. Quantum chemical calculations

Quantum chemical calculations for the seven inhibitors were carried out using Gaussian 09 program package [54]. Density functional theory (DFT) method based on B3LYP approach at level of 6-31G (d) basis sets was applied to optimize molecular geometry, followed by vibrational frequency calculations to ensure that the optimized geometry energy is minimal of the potential energy surface. The solvation effect of water was expressed using polarized continuum model [55]. Based on the optimized geometries, the highest occupied molecular orbital energy, lowest unoccupied molecular orbital energy, energy gap, orbital delocalization index and orbital composition analysis were performed. The orbital delocalization index of HOMO and orbital composition analysis of frontier molecular orbitals were finished by the main function 8 of Multiwfn program [56].

3. Results and discussion

3.1. Chemistry

The seven TSC-ISA-**R** inhibitors used in the present study were synthesized referring the method described previously [48] as outlined in Scheme 1. In brief, 4-(2-methoxy-5-methylphenyl)thiosemicarbazide was firstly synthesized by reaction of 2-isothiocyanato-1-methoxy-4-methylbenzene and hydrazine hydrate (80%) in dichloromethane at room temperature. The synthesis of TSC-ISA-**R** analogues was carried out easily in anhydrous alcohol, using acetic acid as catalyst, by the condensation of 4-(2-methoxy-5-methylphenyl)thiosemicarbazide with 5-substituted indoline-2,3-diones in molar ratio of 1:1 at reflux temperature. The reaction progress was monitored by TLC with ethyl acetate/ petroleum ether (1/1, v/v) as developing solvent. The formed precipitate was collected by centrifugation separation and the target compounds were recrystallized from ethanol or toluene. The yields for the reactions ranged from 52.9% to 91.5%, and all the compounds were characterized by FT-IR, ESI-MS, ^{1}H NMR and ^{13}C NMR (Fig. S1-S4), and their purity was confirmed by elemental analysis. For each target TSC-ISA-**R**, no evidence for the formation of *E-Z* isomers mixture was noted, only the *E* isomer was obtained on the basis of ^{1}H NMR results.

3.2. Inhibitory effects of TSC-ISA-*R* on diphenolase activity of mushroom TYR

The inhibitory effects of TSC-ISA-**R** on mushroom TYR were evaluated in terms of their inhibition against the diphenolase activity of TYR with *L*-DOPA as substrate, referring the assay protocol reported previously [49]. The corresponding parent 5-substituted indoline-2,3-diones were tested in parallel to examine the role of thiosemicarbazido moiety of TSC-ISA-**R** in the inhibition. The progress curves for the catalytic oxidation of *L*-DOPA by mushroom TYR in the presence of different concentrations of TSC-ISA-OCH_3 and TSC-ISA-OCF_3 in PBS containing 3% DMSO are shown in Fig. 1. The inhibitory profiles and inhibition percentages for the other TSC-ISA-**R** are presented in Fig. S5 and Fig. S6 respectively. The values of IC_{50} and inhibition percentage are summarized in Table 1.

It is observed that all TSC-ISA-**R** hybrids displayed inhibitory effects on the catalytic oxidation of *L*-DOPA by mushroom TYR in dose-dependent manner. The inhibition percentages increased distinctly when the concentration of each TSC-ISA-**R** is less than *ca.* 33 μM, and the inhibition almost reached the maximum when the concentration is higher than *ca.* 100 μM (Fig. S6). The enzyme activity was inhibited by 17.66% to 34.42% when the concentration of TSC-ISA-**R** is 33.3 μM, following a decreased order of TSC-ISA-OCH_3 (34.42%) ≈ TSC-ISA-OCF_3 (34.14%) > TSC-ISA-CH_3 (28.41%) > TSC-ISA-Cl (25.12%) > TSC-ISA-F (20.03%) > TSC-ISA-NO_2 (17.74%) ≈ TSC-ISA-H (17.66%). The IC_{50} values of TSC-ISA-**R** on the diphenolase activity of TYR range from 81 to 209 μM, which are higher than that of kojic acid whose IC_{50} value determined in this work is 22 μM. Apparently, the inhibitory competencies of TSC-ISA-**R** are not excellent compared with kojic acid. However, a close correlation of the inhibition ability of TSC-ISA-**R** with the substituent modifications was observed, hence, the substituent effects on the TYR inhibition of these analogues is much worth studying. Moreover, enlightened by the studies of Jung and coworkers [30,32], TSC-ISA-**R** analogues may be worthy of further evaluation as melanogenesis inhibitors since the hydrophobic phenyl and indoline groups possibly allow a better transfer of these molecules across the cell membrane.

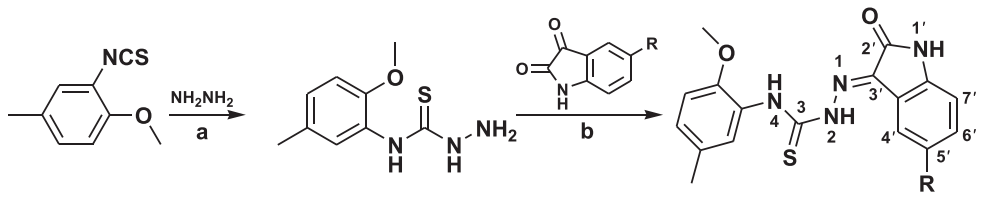

Inhibitor	R
TSC-ISA-H	Hydrogen
TSC-ISA-CH_3	Methyl
TSC-ISA-OCH_3	Methoxyl
TSC-ISA-OCF_3	Trifluoromethoxyl
TSC-ISA-F	Floro
TSC-ISA-Cl	Chloro
TSC-ISA-NO_2	Nitro

Scheme 1. Synthetic procedures for isatin-thiosemicarbazone inhibitors. Reagents and conditions: (a) hydrazine hydrate, 2-isothiocyanato-1-methoxy-4-methylbenzene, dichloromethane, r.t. 120 min; (b) 4-(2-methoxy-5-methylphenyl)thiosemicarbazide, 5-substituted indoline-2,3-dione, ethanol, acetic acid (3 drops), room temperature, reflux, 240 min.

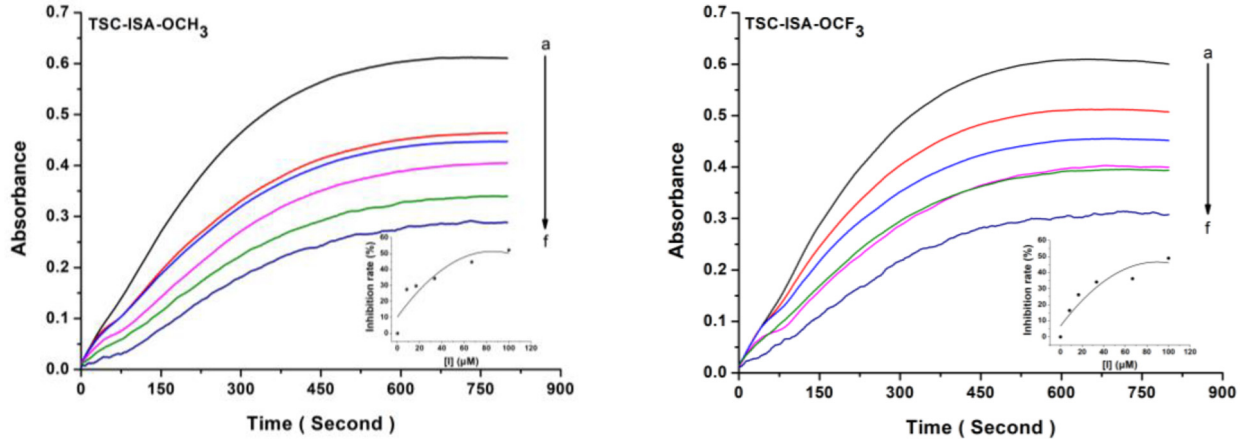

Fig. 1. Progress curves for the catalytic oxidation of *L*-DOPA by TYR in the presence of different concentrations of TSC-ISA-OCH_3 and TSC-ISA-OCF_3 in PBS containing 3% DMSO (v/v). The inset is the plot of inhibition percentage versus concentration of inhibitor. The concentrations of inhibitor for curves a-f are 0, 8.33, 16.67, 33.33, 66.67 and 100 μM, respectively. The concentration of *L*-DOPA is 0.50 mM.

Table 1
Values of IC_{50} and inhibition rate of each TSC-ISA-**R** on mushroom TYR for the catalytic oxidation of *L*-DOPA.

Inhibitor	IC_{50} (μM)	Inhibition percentage (%)[a]
TSC-ISA-H	114 ± 4	17.66 ± 0.79
TSC-ISA-CH_3	209 ± 7	28.41 ± 0.83
TSC-ISA-OCH_3	81 ± 2	34.42 ± 0.85
TSC-ISA-OCF_3	99 ± 3	34.14 ± 0.85
TSC-ISA-F	186 ± 6	20.03 ± 0.62
TSC-ISA-Cl	173 ± 6	25.12 ± 0.76
TSC-ISA-NO_2	120 ± 4	17.74 ± 0.54
ISA-H		−2.76 ± 0.10
ISA-CH_3		−4.42 ± 0.12
ISA-OCH_3		8.48 ± 0.21
ISA-OCF_3		1.63 ± 0.07
ISA-F		−3.00 ± 0.13
ISA-Cl		2.54 ± 0.11
ISA-NO_2		5.52 ± 0.16
Kojic acid	22 ± 2	

[a] Inhibition value for each inhibitor in concentration of 33.33 μM.

Of the examined TSC-ISA-**R** analogues, the unsubstituted one, TSC-ISA-H, showed moderate inhibition capacity (IC_{50} = 114 μM) and the lowest inhibition (17.66% at 33 μM) towards TYR. When the hydrogen atom at C-5 of indoline ring was substituted by strong electronegative halogen atoms, F and Cl, the resulting derivatives TSC-ISA-F and TSC-ISA-Cl severely attenuated the ability to inhibit TYR activity (IC_{50} = 186 and 173 μm, respectively). When the hydrogen atom was substituted by an electron attracting group featuring planar conjugated structure, -NO_2, the resultant TSC-ISA-NO_2 exhibited the inhibitory ability (IC_{50} = 120 μM) comparable to TSC-ISA-H. On the other hand, when substituted by an electron donating group, -CH_3, the resulting TSC-ISA-CH_3 displayed the poorest inhibition potency (IC_{50} = 209 μM). Interestingly, the replacement of the hydrogen atom at C-5 of indoline ring with -OCH_3 and -OCF_3 greatly improved the inhibitory ability of the resulting derivatives, TSC-ISA-OCH_3 and TSC-ISA-OCF_3. It is seen that both analogues stood out to be most potent inhibitors amongst the seven TSC-ISA-**R** derivatives by virtue of their lowest IC_{50} values (81 μM and 99 μM, respectively) and the highest inhibition percentages (34.42% and 34.12% at 33 μM, respectively). Additionally, the corresponding parent 5-substituted isatins exhibited quite weak or even no inhibitory effects on TYR under the same conditions. These observations suggest that TSC-ISA-**R** can inhibit the TYR activity in different degrees, and the thiosemicarbazido moiety is critical for the inhibition, which is in agreement with the prevailing inference claimed in the previous studies. In

this sense, the 5-substituted isatin moiety of each TSC-ISA-**R** is expected to play a regulatory role in the inhibition against TYR.

3.3. Inhibition kinetics of TSC-ISA-*R* on mushroom TYR

Fig. 2 depicts the relationships between the TYR activity and concentration in the presence of different concentrations of TSC-ISA-OCH_3 and TSC-ISA-OCF_3 with constant concentration of *L*-DOPA in 0.5 mM. The graphics corresponding to the other TSC-ISA-**R** analogues were arranged in Fig. S7. The results demonstrate that the seven TSC-ISA-**R** inhibitors behaved in the same manner, specifically, for each TSC-ISA-**R** the plot of the remaining TYR diphenolase activity versus the concentrations of TYR gives a family of straight lines which all go through the origin of the coordinate system. Increasing the concentrations of each TSC-ISA-**R** results in the decline in the slope of the lines, thus revealing that the inhibition against TYR for the catalytic oxidation of *L*-DOPA by the investigated TSC-ISA-**R** analogues is reversible. The results also indicate that the substituent modifications did not alter the inhibition mode of the resultant derivatives towards TYR.

The inhibitory type of each TSC-ISA-**R** was further determined by the well-known Lineweaver-Burk double reciprocal plots based on the inhibitory results. The plots of $1/V$ versus $1/[S]$ for the two most potent TYR inhibitors, TSC-ISA-OCH_3 and TSC-ISA-OCF_3, are presented in Fig. 3, and for the others are arranged in Fig. S8. It is observed that the double-reciprocal plots roughly yield a group of straight lines with different slopes for each inhibitor. As for TSC-ISA-CH_3, TSC-ISA-F, TSC-ISA-NO_2 and TSC-ISA-OCF_3, the lines intersect one another in the second quadrant, and the values of K_M increase but V_{max} decrease with the increasing concentrations of each inhibitor, respectively. As for TSC-ISA-H and TSC-ISA-OCH_3, the respective line intersects one another in the third quadrant, and the corresponding K_M and V_{max} vary reversely with their concentration increase. These results indicate that TSC-ISA-**R** inhibited TYR in a competitive-uncompetitive mixed-type manner, so, each of TSC-ISA-**R** tended to combine with both free TYR and TYR-*L*-DOPA complex forming binary TYR-TSC-ISA-**R** and ternary TYR-*L*-DOPA-TSC-ISA-**R** complexes, respectively [24]. Thus, the interactions between each TSC-ISA-**R** and TYR were not independent of the interactions between *L*-DOPA and TYR, and therefore the TYR-*L*-DOPA affinity may be affected by the TSC-ISA-**R** binding. In the case of TSC-ISA-Cl, the curves intersect in the second quadrant, but the intersection point is very close to the Y-axis (Fig. S8), which suggests that the inhibition behavior of this compound was somewhat different from those of the other inhibitors, it seems more inclined to inhibit TYR in a competitive pattern.

For mixed-type manner, the inhibition constants for inhibitor binding with the free enzyme (K_I) and with the enzyme-substrate complex (K_{IS}) can be determined by the secondary plot of the slope and the intercept of the curves as a function of the inhibitor concentration, respectively [24]. It is observed from Table 2 that for TSC-ISA-H and TSC-ISA-OCH_3 the values of K_I (48.6 and 28.0 μM) are greater than those of K_{IS} (13.7 and 16.4 μM), but for the other inhibitors the K_I values are about 2-fold lower than the corresponding K_{IS} values. The results suggest that the affinities of both TSC-ISA-H and TSC-ISA-OCH_3 to the TYR-*L*-DOPA complex are stronger than to the free TYR, while the situations for the other inhibitors are just contrary. In general, the replacement of the hydrogen atom at C-5 of indoline ring with **R** leads to decrease of K_I values whereas increase of K_{IS} values, which implies that the substitutions enhanced the affinity of the resultant inhibitors to free TYR but weakened the affinity to TYR-*L*-DOPA complex. Notably, the -OCF_3 substituted inhibitor, TSC-ISA-OCF_3, exhibits the smallest K_I value (11.9 μM), which is indicative of the highest affinity of this inhibitor amongst TSC-ISA-**R** to free TYR. Meanwhile, it can be seen that, for TSC-ISA-OCH_3 and TSC-ISA-OCF_3, the sum of K_I and K_{IS} (44.4 and 31.8 μM, respectively) is lower than those of other inhibitors (47.5–118.5 μM), suggesting that both TSC-ISA-OCH_3 and TSC-ISA-OCF_3 have more potent impacts than the other analogues on TYR. This may account for their highest inhibition effects on the diphenolase activity of TYR observed above.

3.4. Inhibition mechanism of TSC-ISA-*R* on mushroom TYR

3.4.1. Possible complexation of TSC-ISA-*R* with the copper ions in TYR

As discussed above, the TYR from different species is known to have a binuclear copper catalytic center which plays a crucial role in TYR activity [1–6]. Slight change of the center possibly leads to activity loss of the enzyme [57]. Naturally, the two copper ions of TYR become the target of various inhibitors studied. Based on a previous study, the $Cu^{2+} \leftrightarrow Cu^{+}$ redox cycle essential for the catalytic activity of TYR can be blocked by the coordination of inhibitors [23]. TSCs are efficacious chelating agents for transition metal ions by virtue of the potential sulfur and nitrogen donors on the thiosemicarbazido moiety [25], which partly explains why a large number of TSC derivatives have been developed as candidates for TYR inhibition. To examine the possible complexation of TSC-ISA-**R** with the Cu^{2+} ions in mushroom TYR, ESI-MS monitoring for the formation of copper complexes between each TSC-ISA-**R** and TYR in PBS containing 3.0% DMSO (v/v) was conducted.

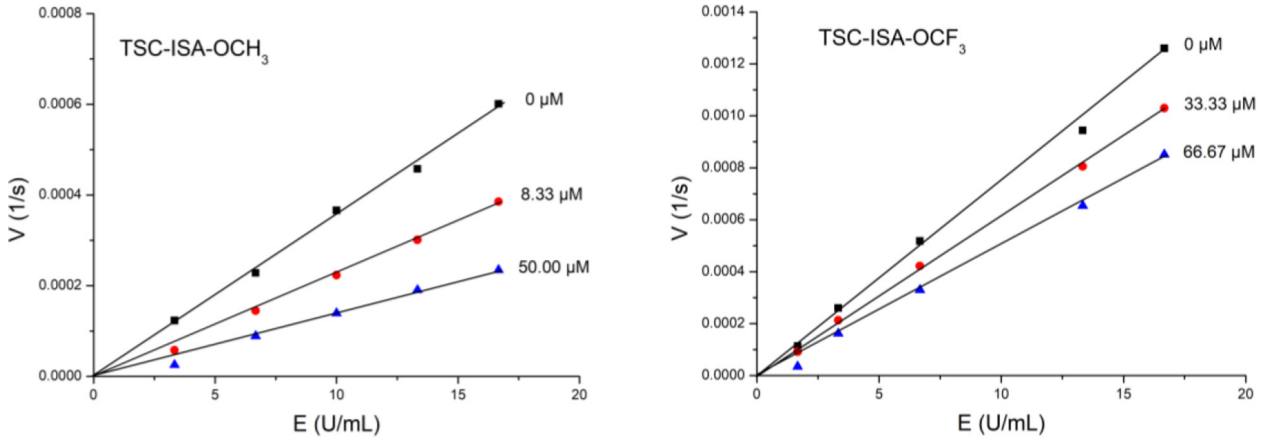

Fig. 2. Relationships between the catalytic activity and concentration of mushroom TYR in the presence of different concentrations of TSC-ISA-OCH_3 and TSC-ISA-OCF_3. The concentration of *L*-DOPA is 0.5 mM.

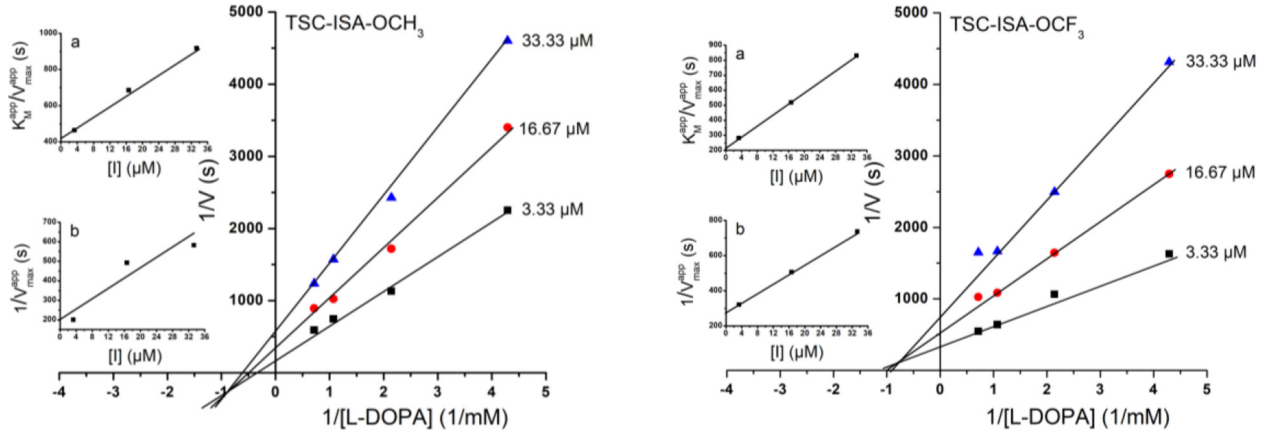

Fig. 3. Lineweaver-Burk plots for the inhibition of TSC-ISA-OCH_3 and TSC-ISA-OCF_3 on mushroom TYR for catalytic oxidation of *L*-DOPA. Insets a and b are the plots of K_M^{app} / V_{max}^{app} and $1/V_{max}^{app}$ versus the concentration of inhibitor, respectively; TYR, 83.3 U/mL.

Table 2
Values of inhibition constants for the binding of each TSC-ISA-**R** with free TYR (K_I) and with TYR-*L*-DOPA complex (K_{IS}).

Inhibitor	K_I (μM)	K_{IS} (μM)	Sum of K_I and K_{IS} (μM)
TSC-ISA-H	48.6 ± 1.0	13.7 ± 0.3	62.3 ± 1.3
TSC-ISA-CH_3	44.6 ± 0.9	73.9 ± 1.6	118.5 ± 2.5
TSC-ISA-OCH_3	28.0 ± 0.7	16.4 ± 0.3	44.4 ± 1.0
TSC-ISA-OCF_3	11.9 ± 0.4	19.9 ± 0.4	31.8 ± 0.8
TSC-ISA-F	16.7 ± 0.5	33.3 ± 0.4	50.0 ± 0.9
TSC-ISA-Cl	16.7 ± 0.5	32.3 ± 0.4	49.0 ± 0.9
TSC-ISA-NO_2	13.5 ± 0.3	34.0 ± 0.4	47.5 ± 0.7

The complexation of each TSC-ISA-**R** with free Cu^{2+} ions was validated by the observations of new bands with λ_{max} at 422–441 nm ascribed to TSC-ISA-**R**-Cu(II) charge transfer (LMCT) transitions in UV–vis spectra (Fig. S9), and the occurrence of the peaks corresponding to mononuclear TSC-ISA-**R**-Cu(II) complexes in 2:1 stoichiometry in ESI-MS (Fig. S10). Contrary to what we had expected, however, almost no TSC-ISA-**R**-Cu(II) species were detected in ESI-MS spectra when each TSC-ISA-**R** was introduced into the TYR solution under the same conditions (Fig. S11). The results indicate that the investigated TSC-ISA-**R** derivatives were hardly engaged in binding the Cu^{2+} ions at the active site of TYR. Thus, it can be inferred that the inhibitory effects of TSC-ISA-**R** on TYR activity were not be achieved by direct complexation with the Cu^{2+} ions in TYR, but, probably by the non-covalent interactions between TSC-ISA-**R** and TYR molecules. To gain more information on the interactions of TSC-ISA-**R** with mushroom TYR, fluorescence and FT-IR spectroscopy analyses were further performed.

*3.4.2. Spectrofluorimetric analysis of the interactions between TSC-ISA-**R** and mushroom TYR*

Fig. 4 depicts the impacts of the presence of TSC-ISA-OCH_3 and TSC-ISA-OCF_3, as well as the corresponding parent 5-substituted isatins in different concentrations on the intrinsic fluorescence of mushroom TYR (others shown in Fig. S12). The results indicate that TYR in the aqueous medium emitted strong fluorescence with the maximum wavelength at 340 nm when excited by 280 nm light, and the fluorescence profiles of TSC-ISA-**R** did not overlap with that of TYR. With gradual addition of each tested TSC-ISA-**R**, the fluorescence intensity of TYR decreased dramatically, revealing an order of quenching degree as TSC-ISA-NO_2 > TSC-ISA-OCH_3 > TSC-ISA-OCF_3 > TSC-ISA-Cl > TSC-ISA-CH_3 > TSC-ISA-F > TSC-ISA-H. Meanwhile, the increasing concentration of each TSC-ISA-**R** led to 2–5 nm blue shifts of the maximum emission wavelength, amongst the inhibitors the shifts induced by TSC-ISA-OCH_3 and TSC-ISA-OCF_3 were the largest, *ca.* 5 nm. These results indicate that not only direct interactions between TSC-ISA-**R** and TYR occurred, but the interactions perturbed the microenvironment around tyrosine and tryptophan residues of TYR [58]. ISA-**R** analogues can also quench the intrinsic fluorescence of TYR under the same conditions (Fig. S13), but the quenching degree was quite weaker except for that induced by ISA-NO_2. The fluorescence quenching resulted by ISA-NO_2 was much significant over the other 5-substituted isatins, and the quenching degree was comparable to that by TSC-ISA-NO_2. Moreover, no significant peak shifts induced by ISA-**R** were observed.

For each inhibitor, the corresponding fluorescence quenching constant (K_{sv}) and rate constant (K_q) of TYR were calculated by the well-known Stern-Volmer equation based on the results of fluorescence titrations at 30 °C, and given in Table 3.

The K_{sv} values of TSC-ISA-**R** range from 2.37×10^4 to 4.41×10^4 M^{-1}, among the data slightly higher ones corresponding to TSC-ISA-OCH_3 and TSC-ISA-OCF_3 (4.41×10^4 and 3.73×10^4 M^{-1}) are observed, which are in accordance to their inhibition competency (IC_{50} = 81 μM and 99 μM, respectively) against TYR. It was reported that the maximal fluorescence quenching rate constant of diffusion collision for biomacromolecules is about 2.0×10^{10} $M^{-1}{\cdot}s^{-1}$ [59]. A compound is considered to quench the intrinsic fluorescence of biomacromolecules via a static process with the formation of a stable complex if K_q value is greater than 2.0×10^{10} $M^{-1}{\cdot}s^{-1}$ [60]. It is observed from Table 2 that the K_q values of TSC-ISA-**R** are in the range of 2.37×10^{12} to 4.24×10^{12} $M^{-1}{\cdot}s^{-1}$, which are comparable each other and all larger than 2.0×10^{10} $M^{-1}{\cdot}s^{-1}$, thus, it is believed that static quenching was dominant in the interactions between TSC-ISA-**R** and TYR, and each of TSC-ISA-**R** was associated with TYR forming a TSC-ISA-**R**-TYR complex. As for ISA-**R**, static fluorescence quenching processes with the formation of ISA-**R**-TYR complexes are also concluded. The K_{sv} and K_q values calculated are in the range of 2.14×10^3 to 2.49×10^4 $L{\cdot}mol^{-1}$ and 2.14×10^{11} to 2.49×10^{12} $M^{-1}{\cdot}s^{-1}$, respectively, which are lower than the corresponding data of TSC-ISA-**R**. It is noteworthy that K_{sv} and K_q values of ISA-NO_2 are 2.49×10^4 M^{-1} and 2.49×10^{12} $M^{-1}{\cdot}s^{-1}$, respectively, which are amongst ISA-**R** the largest and comparable to the corresponding values of TSC-ISA-NO_2 (K_{sv} = 4.24×10^4 M^{-1}, K_q = 4.24×10^{12} $M^{-1}{\cdot}s^{-1}$). This result suggests that, for TSC-ISA-NO_2, the -ISA-NO_2 moiety dominated the fluorescence quenching process, and the binding action of TSC-ISA-NO_2 with TYR and TYR-*L*-DOPA complex was probably different from the other TSC-ISA-**R** analogues.

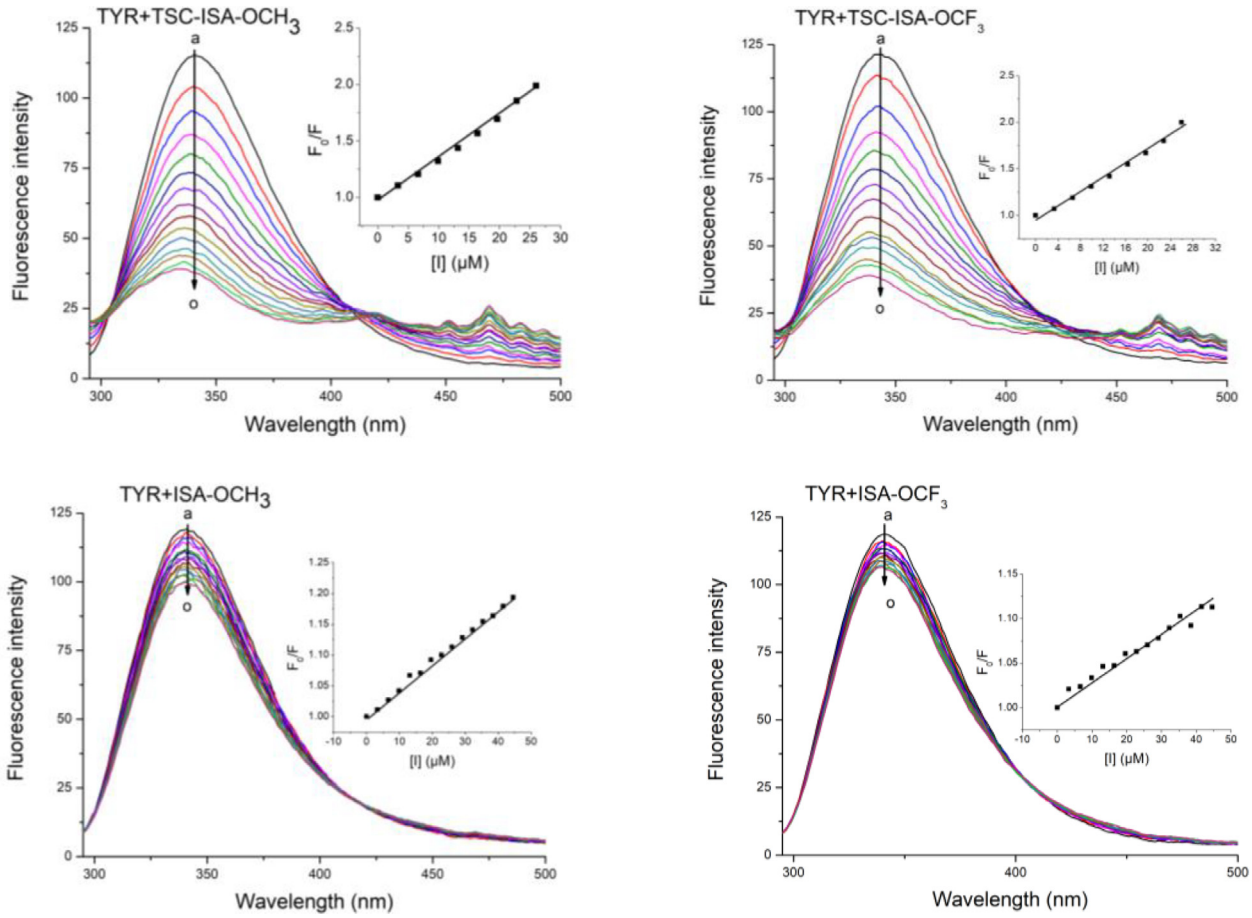

Fig. 4. Effects of the increasing concentrations of TSC-ISA-OCH_3 and TSC-ISA-OCF_3 as well as ISA-OCH_3 and ISA-OCF_3 on the intrinsic fluorescence of mushroom TYR in PBS containing 3% DMSO (v/v). The inhibitor concentrations for curves a to o vary from 0 to 46.48 μM with an interval of 3.32 μM. The inset is the corresponding Stern-Volmer plot. TYR, 83.3 U/mL; λ_{ex} = 280 nm.

Table 3
Calculated fluorescence quenching parameters of TSC-ISA-**R** on TYR, and binding constant and number of binding site of TYR with each TSC-ISA-**R**.

Inhibitor	K_{sv} (M^{-1})	K_q ($M^{-1}\cdot s^{-1}$)	n	K_a (M^{-1})
TSC-ISA-H	$(2.37 \pm 0.11) \times 10^4$	$(2.37 \pm 0.11) \times 10^{12}$	0.97 ± 0.01	$(1.58 \pm 0.04) \times 10^4$
TSC-ISA-CH_3	$(3.04 \pm 0.17) \times 10^4$	$(3.04 \pm 0.17) \times 10^{12}$	1.07 ± 0.01	$(6.11 \pm 0.25) \times 10^4$
TSC-ISA-OCH_3	$(4.41 \pm 0.16) \times 10^4$	$(4.41 \pm 0.16) \times 10^{12}$	1.14 ± 0.01	$(1.73 \pm 0.08) \times 10^5$
TSC-ISA-OCF_3	$(3.73 \pm 0.19) \times 10^4$	$(3.73 \pm 0.19) \times 10^{12}$	1.25 ± 0.01	$(5.48 \pm 0.14) \times 10^5$
TSC-ISA-F	$(2.84 \pm 0.11) \times 10^4$	$(2.84 \pm 0.11) \times 10^{12}$	1.06 ± 0.01	$(5.00 \pm 0.12) \times 10^4$
TSC-ISA-Cl	$(3.15 \pm 0.13) \times 10^4$	$(3.15 \pm 0.13) \times 10^{12}$	1.08 ± 0.01	$(7.65 \pm 0.27) \times 10^4$
TSC-ISA-NO_2	$(4.24 \pm 0.20) \times 10^4$	$(4.24 \pm 0.20) \times 10^{12}$	1.06 ± 0.01	$(8.26 \pm 0.26) \times 10^4$
ISA-H	$(2.99 \pm 0.12) \times 10^3$	$(2.99 \pm 0.12) \times 10^{11}$	0.89 ± 0.01	$(9.88 \pm 0.28) \times 10^2$
ISA-CH_3	$(2.45 \pm 0.11) \times 10^3$	$(2.45 \pm 0.11) \times 10^{11}$	0.87 ± 0.01	$(6.93 \pm 0.17) \times 10^2$
ISA-OCH_3	$(4.33 \pm 0.18) \times 10^3$	$(4.33 \pm 0.18) \times 10^{11}$	1.00 ± 0.01	$(4.45 \pm 0.12) \times 10^3$
ISA-OCF_3	$(2.58 \pm 0.12) \times 10^3$	$(2.58 \pm 0.12) \times 10^{11}$	0.83 ± 0.01	$(4.81 \pm 0.14) \times 10^2$
ISA-F	$(2.23 \pm 0.07) \times 10^3$	$(2.23 \pm 0.07) \times 10^{11}$	0.98 ± 0.01	$(3.17 \pm 0.13) \times 10^2$
ISA-Cl	$(2.14 \pm 0.10) \times 10^3$	$(2.14 \pm 0.10) \times 10^{11}$	0.94 ± 0.01	$(1.17 \pm 0.08) \times 10^3$
ISA-NO_2	$(2.49 \pm 0.13) \times 10^4$	$(2.49 \pm 0.13) \times 10^{12}$	1.05 ± 0.01	$(3.94 \pm 0.14) \times 10^4$

For the static quenching interaction, the apparent binding constant (K_a) and the number of binding sites (n) between each TSC-ISA-**R** and TYR were calculated by Eq. (2) [52], assuming that there are similar and independent sites in a TYR molecule. It is seen from Table 2 that the value of n for each TSC-ISA-**R** is near 1, which suggests that each TSC-ISA-**R** combined with TYR through one binding site. The K_a values for TSC-ISA-**R** binding with TYR range from 1.58×10^4 to 5.48×10^5 M^{-1} at 30 °C, among which the highest ones corresponding to TSC-ISA-OCH_3 and TSC-ISA-OCF_3 were observed, in good agreement with their minimum sum of K_I and K_{IS} presented in Table 2. The results are suggestive of the strongest affinity of the two inhibitors to TYR, which are again consistent with their most potent inhibitory effects on TYR activity. For the other TSC-ISA-**R** analogues, it was not possible, however, to correlate the values of K_a with their inhibitory competency directly, similar to the observations reported for other TYR inhibitors [58,61]. In comparison, the K_a values of ISA-**R** binding with TYR (3.17×10^2 – 3.94×10^4 M^{-1}) were likewise less than those of the corresponding TSC-ISA-**R**. Remarkably, an exception was observed for TSC-ISA-OCF_3 whose K_a value is one order of magnitude higher than those of the other TSC-ISA-**R** analogues, whereas the K_a value of ISA-OCF_3 is smaller, only 4.81×10^2 M^{-1}. This result indicates that

TSC-ISA-OCF_3 combined more strongly than the other TSC-ISA-**R** with TYR, the thiosemicarbazido moiety but -ISA-OCF_3 made a major contribution to the binding. In contrast, the calculated K_a of ISA-NO_2 is 3.94 × 10^4 M^{-1}, a value being comparable to that of TSC-ISA-NO_2 (K_a = 8.26 × 10^4 M^{-1}), which implies that the -ISA-NO_2 moiety seemed to have a major contribution to the combination of TSC-ISA-NO_2 with TYR.

Such binding may induce the conformation changes of TYR, which probably hindered the channel for *L*-DOPA access to the active center, and accordingly inhibited TYR activity. Synchronous fluorescence spectroscopy has been widely used in the study of protein-molecule interactions, and it can provide information about the molecular environment in the vicinity of the fluorophore functional groups, as well as identify possible conformational changes on the protein structure [38,62,63]. The information in relation to the variations of microenvironment around the tyrosine and tryptophan residues of TYR can be obtained from the synchronous fluorescence spectra of TYR when the wavelength interval (Δλ) between excitation and emission wavelength was set at 15 nm and 60 nm, respectively [62]. Thereby, this technique was used to verify the possibility underlying the interactions between TSC-ISA-**R** and TYR in the following experiments.

Fig. S14 presented in the supplementary materials illustrates the effects of the increasing concentrations of each TSC-ISA-**R** on the synchronous fluorescence of these fluorophores in mushroom TYR. It is shown that the fluorescence intensity of tyrosine residues (Δλ = 15 nm) was enhanced substantially with the addition of the tested TSC-ISA-**R** except for TSC-ISA-NO_2. Meanwhile, 2–14 nm of red shifts at the maximum emission wavelengths were observed when the concentration of each inhibitor was increased by 38.46 μM. An exception was observed for TSC-ISA-NO_2 which attenuated the fluorescence intensity accompanied by only 2 nm of red shift. Anyway, the results suggest that each TSC-ISA-**R** interacted with TYR molecules disturbing the microenvironment in the vicinity of tyrosine residues, and decreased the hydrophobicity of the amino acid residues near tyrosine residues to different extent. In contrast, the addition of each TSC-ISA-**R** resulted in significant fluorescence quenching of tryptophan residues (Δλ = 60 nm), however, no noticeable shift at the maximum emission peaks was observed. These results indicate that the presence of each TSC-ISA-**R** hardly perturbed the microenvironment around tryptophan residues [38]. Thus, it could be supposed that each TSC-ISA-**R** may locate closer to the tyrosine residues than to the tryptophan residues. Moreover, the inhibitor binding has affected the molecular conformation of TYR, as indicated previously for β-enamino thiosemicarbazide derivatives [64].

3.4.3. FT-IR analysis of the interactions between TSC-ISA-*R* and tyrosinase

Infrared spectroscopy is a useful technique to gain insight into the secondary structure changes of proteins in solution and in biological systems [65]. As shown in Fig. 5, a wide band centered at 1655 cm^{-1}, assigned as the characteristic absorption of the amide I band of TYR arising mainly from amide C═O stretching vibration of the protein backbone [66], was observed from the spectrum of the free TYR. The presence of TSC-ISA-F, TSC-ISA-Cl, and TSC-ISA-NO_2 greatly shifted the absorption of the amide I band to low wavenumber (Δσ = 23, 25 and 26 cm^{-1}, respectively, See Table S1) and significantly enhanced the intensity (about 3–4 fold). It was reported that TYR is predominately α-helix in nature [67]. The red shift of the absorption band is suggestive of lengthening of the α-helix chain [68]. On the contrary, in the presence of TSC-ISA-H and TSC-ISA-CH_3, the absorption intensity of the amide I band was markedly attenuated along with a little shift of the characteristic peak to high wavenumber. Remarkably, the presence of TSC-ISA-OCH_3 and TSC-ISA-OCF_3 almost resulted in the disappearance of the absorption of the amide I band located at 1655 cm^{-1}. Moreover, in the case of TSC-ISA-OCF_3, a faint but discernible band centered at 1676 cm^{-1}, probably attributed to β-turn structure, was observed in the spectrum. These observations indicate that the tested TSC-ISA-**R** interacted with TYR and induced conformational changes and stability decrease of the enzyme to different extent [69]. Both TSC-ISA-H and TSC-ISA-CH_3 decreased the α-helix content of TYR, and both TSC-ISA-OCH_3 and TSC-ISA-OCF_3 even led to the loss of main secondary structure elements [66,69].

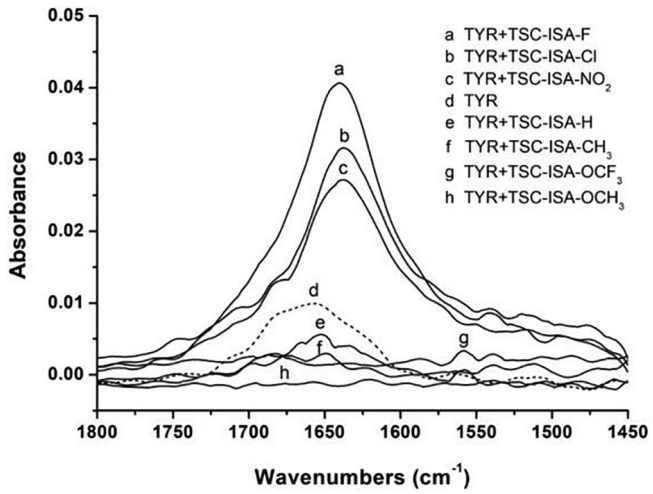

Fig. 5. Effects of TSC-ISA-**R** on the FT-IR spectra of TYR in PBS containing 3% DMSO (v/v).

It is known that the ligand–protein binding process is mainly driven by four non-covalent interaction forces including hydrophobic interaction, van der Waals forces, hydrogen bonding and electrostatic forces. The crystallographic structure of TYR revealed that TYR has two distinct combination sites for binding with substrate and inhibitors. One is the binuclear copper ions active centre and the other is the hydrophobic enzyme pocket active site adjoining the binuclear copper active site [1,4,6,70]. TSC-ISA-**R** analogues feature lipophilic phenyl and indoline groups, which could facilitate TSC-ISA-**R** molecules to approach the lipophilic surface of TYR through hydrophobic interaction and Van der Wals forces, thus hindering the entry of substrate to the copper active center, and therefore influencing the TYR activity. Furthermore, the amino or/and carbonyl groups of TSC-ISA-**R** might form potential intermolecular hydrogen bonding with the sulfhydryl, amino, carboxyl or hydroxyl groups near the active center [70], also possibly with the oxygen bridges linking the two copper sites of TYR [8,18], thus further affecting the TYR catalysis.

3.4.4. Interactions between TSC-ISA-*R* with L-DOPA

Besides the TSC-ISA-**R** binding with free TYR and TYR-*L*-DOPA complex can directly inhibit the diphenolase activity of TYR, the possible interactions between TSC-ISA-**R** with substrate *L*-DOPA may indirectly exert their inhibitory effects on TYR activity. In order to validate this possibility, further investigations were carried out under the same conditions using fluorescence titrations as well as ESI-MS.

Fig. 6 displays the fluorescence changes of *L*-DOPA in PBS containing 3% DMSO at 30 °C in the presence of different concentrations of TSC-ISA-OCH_3 and TSC-ISA-OCF_3 as well as ISA-OCH_3 and ISA-OCF_3 (others shown in Fig. S15 and S16). As shown in the figures, *L*-DOPA in the aqueous medium yielded strong fluorescence with the maximum wavelength at 317 nm when excited by

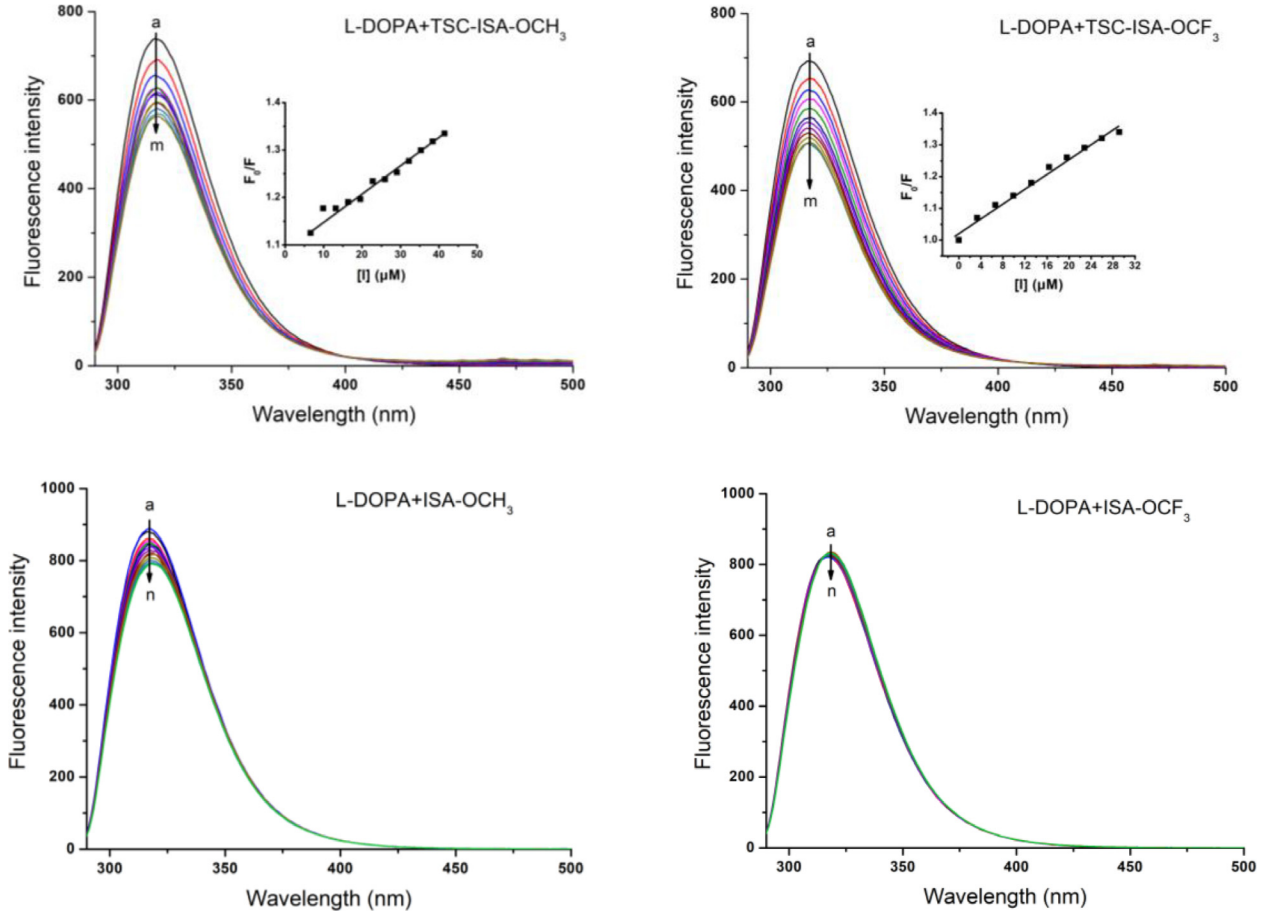

Fig. 6. Effects of the increasing concentration of TSC-ISA-OCH_3 and TSC-ISA-OCF_3 as well as ISA-OCH_3 and ISA-OCF_3 on the fluorescence of *L*-DOPA in PBS containing 3% DMSO (v/v). The concentrations of TSC-ISA-OCH_3 and TSC-ISA-OCF_3 as well as ISA-OCH_3 and ISA-OCF_3 for curves a to m and a to n vary from 0 to 39.84 μM and 0 to 43.16 μM with an interval of 3.32 μM, respectively. The concentration of *L*-DOPA is 0.50 mM. The inset is the corresponding Stern-Volmer plot. λ_{ex} = 280 nm.

280 nm light, and the overlapping of the fluorescence profiles of the inhibitors with that of *L*-DOPA was not observed. Similar to the effects of these inhibitors on the intrinsic fluorescence of mushroom TYR, the increasing concentrations of TSC-ISA-**R** significantly quenched the fluorescence of *L*-DOPA, while the shift of the emission peaks was hardly observed. ISA-**R** except for ISA-NO_2 had tiny impacts on the fluorescence. The fluorescence quenching constant K_{sv} and apparent binding constants K_a of each TSC-ISA-**R** were calculated according to the Eqs. (2) and (3), respectively, and summarized in Table 4. It can be seen that the K_{sv} values are comparable to those of TSC-ISA-**R** on TYR, whereas K_a values, except for that of TSC-ISA-H (K_a = 5.62 × 10^4 M^{-1}), are much lower than those of TSC-ISA-**R** binding with TYR (Table 4).

The binding of each TSC-ISA-**R** with *L*-DOPA was further confirmed by the formation of TSC-ISA-**R**-*L*-DOPA complexes detected in ESI-MS spectra (Fig. 7 and Fig. S17). These results indicate that TSC-ISA-**R** not only interacted directly with TYR, but also with the substrate *L*-DOPA under the same conditions.

Table 4
Calculated fluorescence quenching parameters of TSC-ISA-**R** for *L*-DOPA, and binding constants for each TSC-ISA-**R** with *L*-DOPA.

Inhibitor	K_{sv} (M^{-1})	K_a (M^{-1})
TSC-ISA-H	(1.34 ± 0.06) × 10^4	(5.62 ± 0.13) × 10^4
TSC-ISA-CH_3	(7.40 ± 0.12) × 10^3	(6.10 ± 0.18) × 10^2
TSC-ISA-OCH_3	(6.96 ± 0.21) × 10^3	(1.76 ± 0.05) × 10^2
TSC-ISA-OCF_3	(1.13 ± 0.02) × 10^4	(9.12 ± 0.17) × 10^2
TSC-ISA-F	(1.01 ± 0.01) × 10^4	(7.10 ± 0.13) × 10^2
TSC-ISA-Cl	(1.29 ± 0.03) × 10^4	(8.39 ± 0.15) × 10^3
TSC-ISA-NO_2	(1.25 ± 0.03) × 10^4	(1.82 ± 0.09) × 10^3

Taken above results together, it could be postulated that three potential interactions were probably involved in the inhibition of TSC-ISA-**R** on TYR activity. One is the non-covalent binding of TSC-ISA-**R** with TYR through hydrophobic interaction and Van der Wals forces, which could block the combination of *L*-DOPA and the binuclear copper active site of TYR. This interaction may merely interfere with the coordination bonds formed by Cu^{2+} with amino acid residues in TYR and the non-covalent interactions between the coppers and residues, similar to other TYR inhibitors [3]. The thiosemicarbazido moiety of TSC-ISA-**R** played a crucial role in the interaction. The isatin moiety may act as an auxiliary functionality which bound the hydrophobic protein pocket through hydrophobic interaction and Van der Wals forces facilitating the thiosemicarbazide moiety to approach the hydrophobic domain surrounding the enzyme active center. The second one is the binding of TSC-ISA-**R** to the *L*-DOPA-TYR complex, which may decrease the affinity of the substrate *L*-DOPA to TYR, and therefore inhibit the TYR activity. The third one is the competitive binding of TSC-ISA-**R** with the substrate *L*-DOPA, which may impede the access of *L*-DOPA to the copper catalytic site of TYR, and thus indirectly inhibited the diphenolase activity of TYR. Such three interactions may act independently or collaboratively to exert inhibitory effects of TSC-ISA-**R** on TYR activity.

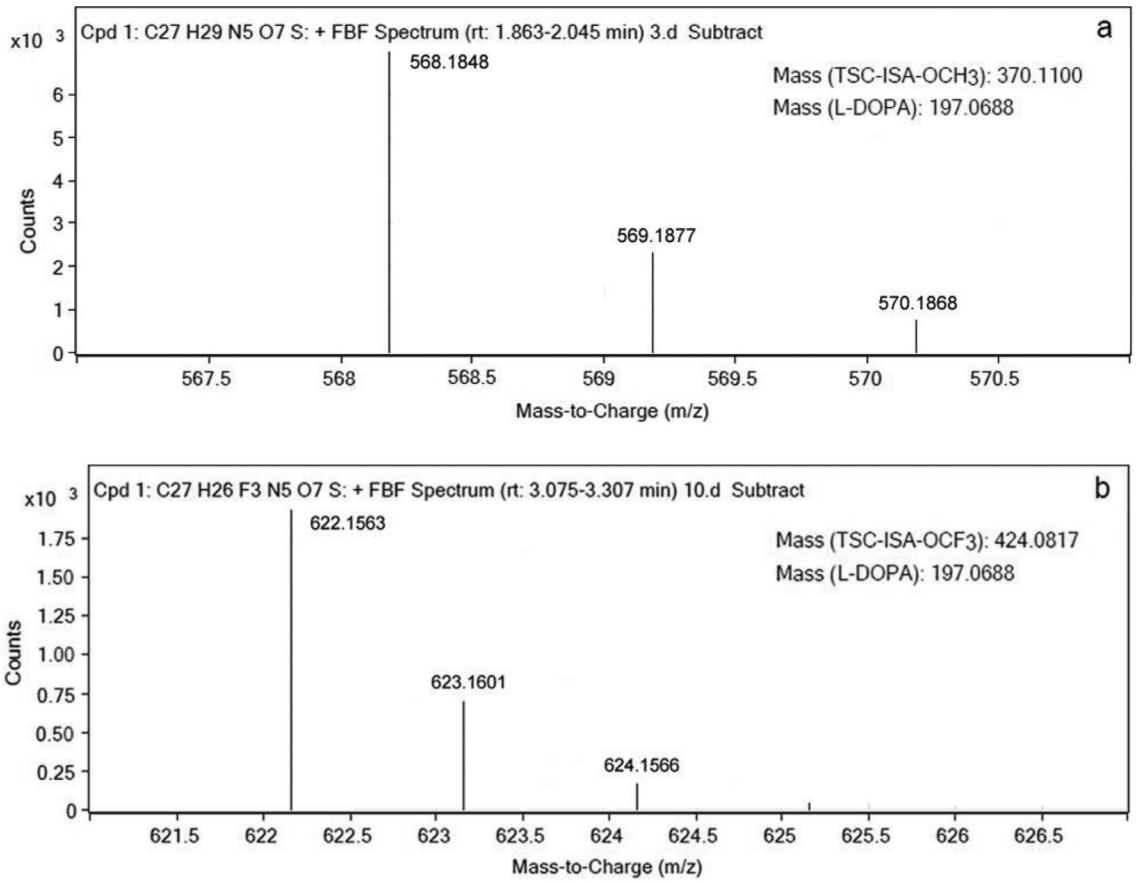

Fig. 7. ESI-MS spectra for the mixture of *L*-DOPA and TSC-ISA-OCH_3 (a), and TSC-ISA-OCF_3 (b) in PBS buffer containing 3% DMSO (v/v).

*3.5. Considerations of substituent effects of TSC-ISA-**R** on the inhibition against TYR activity*

Inspection of the above experimental results reveals a roughly positive correlation of the inhibition effects of TSC-ISA-**R** with their affinities to TYR and *L*-DOPA-TYR complex (Tables 2 and 3). The investigated TSC-ISA-**R** analogues in this study share the identical molecular skeleton but only differ in the substituents (**R**) at C-5 of indoline ring (Scheme 1). Therefore, it seems safe to assume that the **R** groups were responsible for the difference between TSC-ISA-**R** in the association with TYR and *L*-DOPA-TYR complex, and then in the inhibition against TYR. In general, four non-covalent interaction forces including hydrophobic interaction, van der Waals forces, hydrogen bonding and electrostatic forces are known to mainly contribute to the ligand–protein binding, as mentioned above. The electrostatic attraction of TSC-ISA-**R** to TYR could be neglected due to weak dissociation and protonation of each inhibitor in PBS at pH 6.80 employed in this work. Thus, hydrophobic interaction, van der Waals forces and hydrogen bonding may be involved in the combination of TSC-ISA-**R** and TYR. The attributes of –**R** substituents including steric hindrance, lipophilicity, spatial configuration, and electronic effects, etc. may have different impacts on these non-covalent interaction forces, and accordingly on the inhibitory efficacy of TSC-ISA-**R** towards TYR.

The typical physico-chemical parameters of each TSC-ISA-**R** inhibitor calculated theoretically by ACD/Labs software [71], and the Hammett values of **R** substituent groups determined by Hammett methodology [72] were summarized in Table 5.

The molar volume of TSC-ISA-**R** shown in Table 5 ranges from 250.2 to 286.7 M^{-1} with TSC-ISA-OCF_3 showing the largest and TSC-ISA-H the smallest. It can be seen from these data that the variation of the substituents at C-5 of indoline ring can change the molecular size of the resulting TSC-ISA-**R** in different degrees. From the view of steric hindrance, large size of substituents may generally lead to the blocking of inhibitor molecules to approach the hydrophobic domain of TYR active center, thus possibly hindering the association of the inhibitor with TYR, and further affecting its inhibitory effect on TYR activity [35,73,74]. In this regard, the affinity of TSC-ISA-OCF_3 to TYR and its inhibitory competency should be the lowest but TSC-ISA-H be the highest. However, this inference is inconsistent with the experimental results (Tables 1–3), which suggests that the **R**-resulted size alterations of TSC-ISA-**R** molecules were not significant for their TYR inhibition, and other more important factors may underlie the difference in TYR affinity and inhibition efficacy between TSC-ISA-**R** analogues. Furthermore, these substituents probably did not participate in the interactions of TSC-ISA-**R** with TYR and its substrate complex.

Table 5
Typical physico-chemical parameters of the inhibitor and substituent group **R**.

Inhibitor	$logD_{6.8}$	Molar volume (M^{-1})	σ_{para}
TSC-ISA-H	3.34	250.2	0
TSC-ISA-CH_3	3.80	265.4	−0.17
TSC-ISA-OCH_3	3.51	271.9	−0.27
TSC-ISA-OCF_3	3.43	286.7	0.35
TSC-ISA-F	2.49	253.1	0.062
TSC-ISA-Cl	3.06	259.5	0.23
TSC-ISA-NO_2	2.05	255.5	0.78

The effects of lipophilicity of TYR inhibitors on their inhibitory competency have been extensively studied, and the results indicate that the lipophilicity of substituent groups on a inhibitor

molecule is an important even a determinant factor affecting the inhibitory ability of the inhibitor towards TYR or melanogenesis [22,30]. Lipophilicity is usually expressed as logarithm of the partition coefficient (logP) for non-ionized analytes or logarithm of the distribution coefficient (logD) for ionizable analytes in immiscible liquids [75]. The index $logD_{6.8}$ determined at pH 6.80 was herein used to evaluate the contribution of hydrophobicity and hydrophilicity to the binding of TSC-ISA-**R** analogues with TYR since all relevant measurements was conducted in PBS (pH = 6.80) containing 3% DMSO. It is seen from Table 5 that the substitution of the hydrogen atom at C-5 of indoline ring with -F, -Cl and $-NO_2$ groups resulted in the decrease of $logD_{6.8}$ values, corresponding to the decrease of hydrophobicity of the resulting TSC-ISA-F, TSC-ISA-Cl and TSC-ISA-NO_2. The affinity of the three analogues to TYR caused by hydrophobic interaction and van der Waals forces could be reduced accordingly. On the contrary, the substitution of the hydrogen atom with $-CH_3$, $-OCH_3$ and $-OCF_3$ groups increased $logD_{6.8}$ of the resultant TSC-ISA-CH_3, TSC-ISA-OCH_3 and TSC-ISA-OCF_3, which corresponds to the increase of their hydrophobicity and affinity to TYR. Clearly, the substituent modifications influenced the hydrophobicity of the isatin-TSC hybrids investigated in this study, however, no apparent correlation of the affinities (K_a), and further the inhibitory effects (IC_{50}) of TSC-ISA-**R** on TYR with their $logD_{6.8}$ values were observed. Nevertheless, it can be inferred that moderate values of $logD_{6.8}$, e.g. 3.4–3.5, seem to be more favorable to the interactions between TSC-ISA-**R** and TYR, and thus beneficial to their inhibitory ability.

In addition, the electronic effects of **R** may also exert impacts on the interactions between TSC-ISA-**R** and TYR, and further on the TYR inhibition. The electronic effects of substituents, originally used for the study of the rates and equilibria in different external side-chain reactions of benzene derivatives by the well-known Hammett methodology [72], are mainly composed of a field/inductive component (I) and a resonance (π-electron delocalization) component (R) [76]. The electronic character of the substituents on six-membered ring systems is usually quantified in terms of position according to Hammett values (σ_{meta} or σ_{para}). The σ constant has been chosen as the chemical descriptor and one of the most commonly employed substituent descriptor. More positive values of σ are associated with more electron-withdrawing substituent groups, and *vice versa* [72]. The σ_{para} value of a substituent equals the sum of its field/inductive parameter (σ_I) and resonance parameter (σ_R), *i.e.* $\sigma_{para} = \sigma_I + \sigma_R$ [77]. In the present study, the difference in the π-electron densities on the benzene ring of isatin moiety of TSC-ISA-**R** as a result of substituent effects of **R** could be qualitatively estimated using the reported σ_{para} values of **R**. It is observed from Table 5 that the Hammett σ_{para} values for -H, -CH_3, -OCH_3, -OCF_3, -F -Cl and -NO_2 are 0, −0.17, −0.27, 0.35, 0.062, 0.23 and 0.78, respectively [72]. Obviously, the -NO_2 group is the strongest π-electron acceptor followed by -OCF_3 as evidenced by their positive and relatively large Hammett σ_{para} values. In contrast, the -OCH_3 group is the strongest π-electron donor followed by -CH_3 by virtue of their negative and relatively low σ_{para} values. Accordingly, the π-electron densities on the benzene ring of isatin moiety attached by -NO_2 and -OCF_3 are more deficient but the π-electron densities on the benzene ring appended by -OCH_3 and -CH_3 are richer in comparison with the unmodified TSC-ISA-H. Such electronic effects could further affect the electron density on the secondary amino-N1′ of indoline ring as well as the exocyclic carbonyl O and imino N1 atoms. In this respect, the electron densities on these atoms of TSC-ISA-NO_2 and TSC-ISA-OCF_3 could be decreased, which facilitates the two inhibitors to bind TYR through hydrogen bonding interactions with the secondary amino group as a hydrogen bonding donor. However, the more deficient π-electron densities on the indoline benzene ring of TSC-ISA-NO_2 as a result of the more electron-withdrawing -NO_2 group is likely to be unfavourable to π-π stacking interactions with the aromatic rings in TYR. This may account for the lower affinity of TSC-ISA-NO_2 to TYR ($K_a = 8.26 \times 10^4\ M^{-1}$) than TSC-ISA-$OCF_3$ ($K_a = 5.48 \times 10^5\ M^{-1}$). In contrast, the electron densities on the secondary amino-N1′, the exocyclic carbonyl O and imino N1 atoms of TSC-ISA-OCH_3 and TSC-ISA-CH_3, especially TSC-ISA-OCH_3, could be increased, which may be conducive to the formation of hydrogen bonding with these atoms as hydrogen bond acceptors with TYR. Interestingly, the introduction of similar bulky substituent groups with distinct σ values at C-5 of indoline ring, e.g. -OCH_3 and -OCF_3, can yield similar contribution to improving the inhibitory competency of the resulting inhibitors towards TYR.

In summary, the substituent modifications of C-5 of isatin moiety can alter the characters such as the molecular size, lipophilicity and electron density on the indoline ring of the resulting TSC-ISA-**R** to different extent. These alterations could further affect the affinity of TSC-ISA-**R** to TYR, and therefore their inhibitory effects on TYR activity.

3.6. Theoretical studies

In order to further understand the structural features of TSC-ISA-**R** molecules, DFT calculations were performed at B3LYP level with 6-31G (d) basis sets. The previous study has indicated that the frontier molecular orbitals (FMO) such as the highest occupied molecular orbital (HOMO) and lowest unoccupied molecular orbital (LUMO) can be used to evaluate the reactivity of a molecule [78]. The value of HOMO in a molecule indicates the electron-donating ability of the molecule. The molecule with a higher value of this parameter has a higher chemical reactivity. On the other hand, the LUMO value of a molecule implies the electron-accepting capability of the molecule. The molecule with a smaller value of this parameter has a higher chemical reactivity [79]. The energy gap (ΔE) between HOMO and LUMO can help to characterize the chemical and biological reactivity, and kinetic stability of the molecule [80]. Fig. 8(a)–(g) show the orbital isosurface of frontier molecular orbitals, E_{HOMO}, E_{LUMO} and ΔE of the seven TSC-ISA-**R** molecules. The positive and negative phases are represented in green and blue color respectively.

It can be seen from Fig. 8 that the HOMO of TSC-ISA-OCH_3 is mainly composed of the indolyl ring, oxygen atom of 5′-methoxy and thiourea moiety, which is very different from the other six TSC-ISA-**R** molecules whose HOMO orbitals are principally composed of the phenyl ring, methoxy oxygen atom and thiourea moiety. It is worth noting that the contribution of oxygen atom of 5′-methoxy group to the HOMO of TSC-ISA-OCH_3 is as high as 11.53% (see Table S2), which implies that -OCH_3 substitution at C-5 of indolyl ring is helpful to improve electron-donating ability of HOMO. Apparently, the substituent groups appended at C-5 position of indoline ring affect the electron distribution in HOMO of the inhibitor molecules investigated, which can also be observed from the resulted delocalization degree of the corresponding HOMO. The degree of spatial delocalization of frontier molecular orbitals can be quantitatively characterized by orbital delocalization index (ODI). The smaller ODI indicates the higher degree of orbital delocalization, and *vice versa*. Table 6 presents the ODI values of HOMO in the seven TSC-ISA-**R** molecules. What attracted our attention is that the -OCH_3 substitution substantially decreases the ODI of the resultant TSC-ISA-OCH_3, which implies 5′-OCH_3 significantly increases the orbital delocalization degree of HOMO in TSC-ISA-OCH_3.

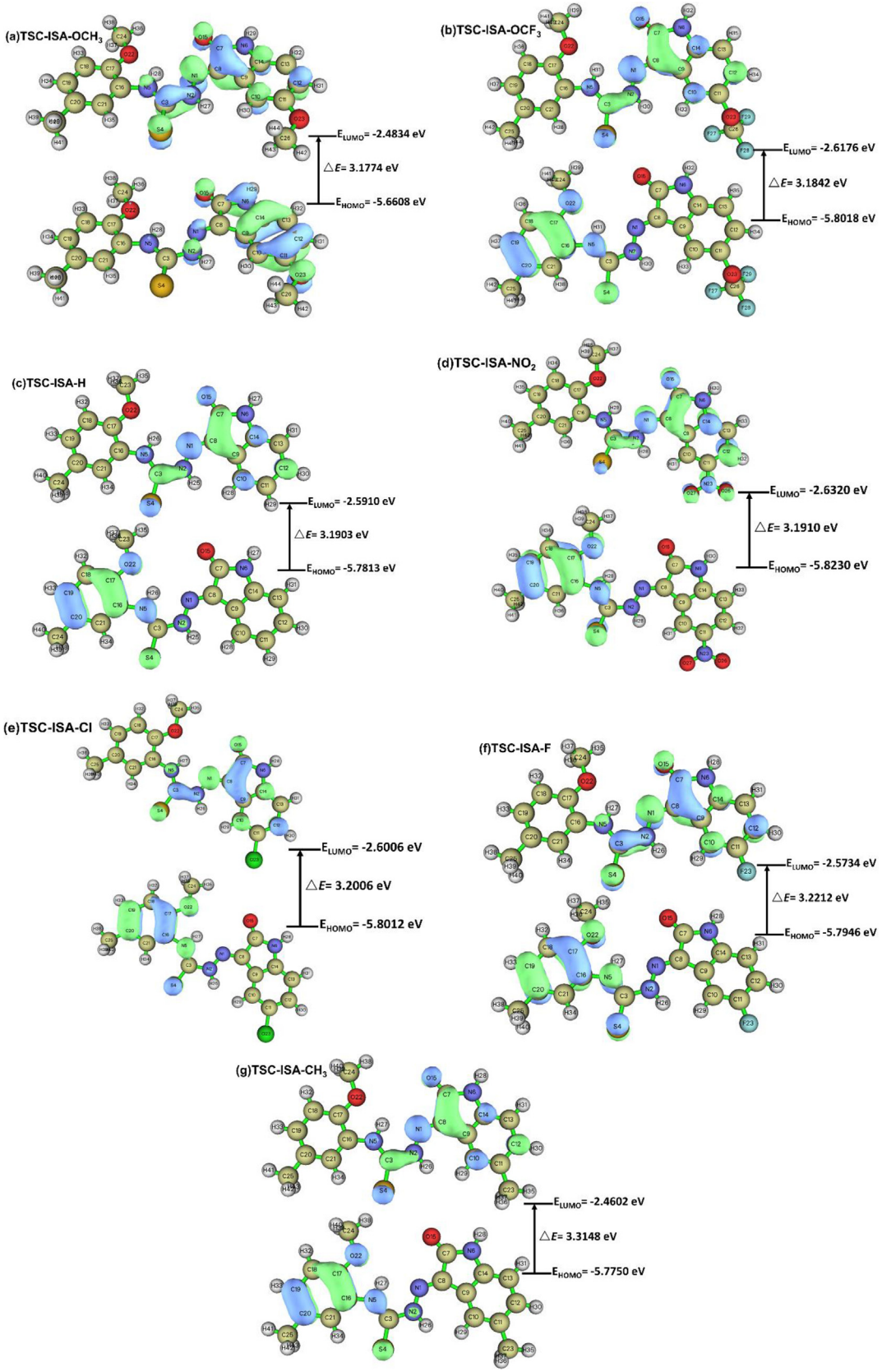

Fig. 8. Orbital isosurface of frontier molecular orbitals, E_{HOMO}, E_{LUMO} and energy gap (ΔE) of seven TSC-ISA-R compounds. (a) TSC-ISA-OCH_3, (b) TSC-ISA-OCF_3, (c) TSC-ISA-H, (d) TSC-ISA-NO_2, (e) TSC-ISA-Cl, (f) TSC-ISA-F, and (g) TSC-ISA-CH_3.

Table 6
Orbital delocalization index of HOMO of the seven TSC-ISA-**R** inhibitors.

	TSC-ISA-OCH_3	TSC-ISA-OCF_3	TSC-ISA-H	TSC-ISA-NO_2	TSC-ISA-Cl	TSC-ISA-F	TSC-ISA-CH_3
ODI	8.64	11.76	11.44	11.95	11.67	11.45	10.90

In the case of LUMO, the orbital composition is similar, namely, the electrons are distributed entirely over the indolyl ring and thiourea moiety in the title molecules. An except was observed for TSC-ISA-NO_2, specifically, the contribution of the 5′-NO_2 group to LUMO of TSC-ISA-NO_2 is 14.15%, while the contributions of the other substituents to LUMO composition of the corresponding molecule are less than 0.5% (Table S3).

The values of LUMO-HOMO energy gap calculated for the title molecules were shown in Fig. 8. It can be observed that ΔE increases in the following order: TSC-ISA-OCH_3 < TSC-ISA-OCF_3 < TSC-ISA-H < TSC-ISA-NO_2 < TSC-ISA-Cl < TSC-ISA-F < TSC-ISA-CH_3, which almost accords with the order of IC_{50} values obtained from the inhibitory assays. Previous studies have shown that the lower ΔE of a molecule facilitates charge transfer interaction within the molecule, contributing to a high capacity of its bioactivity [81,82]. The lowest ΔE in TSC-ISA-OCH_3 reveals the significant degree of charge transfer interactions taking place in the molecule, and hence it is favourable for the enhanced chemical as well as biological activity of this molecule.

4. Conclusions

In this study, seven new isatin-thiosemicarbazones with different substituents (**R**) attached at the C-5 position of indoline ring, TSC-ISA-**R** (**R** = -H, -CH_3, -OCH_3, -OCF_3, -F, -Cl and -NO_2), were synthesized and evaluated as TYR inhibitors. Their inhibitory competency was investigated by examining the inhibition against the diphenolase activity of mushroom TYR with *L*-DOPA as substrate, using spectroscopic techniques. TSC-ISA-**R** analogues displayed different inhibitory effects on TYR activity with IC_{50} values ranging from 81 to 209 μM. In comparison, -OCH_3 and -OCF_3 substitutions improved the inhibitory effects, while -CH_3, -F and -Cl substitutions decreased the inhibitory efficacy. The kinetic analyses showed that TSC-ISA-**R** were reversible and mixed type inhibitors on this enzyme. A roughly positive correlation of the inhibition effects of TSC-ISA-**R** on TYR activity with their affinities to TYR was observed. The mechanism study indicated that three potential interactions including the non-covalent TSC-ISA-**R** binding with free TYR, TYR-*L*-DOPA complex, and with substrate *L*-DOPA were probably involved in the inhibition of TSC-ISA-**R** against TYR. The combination of TSC-ISA-**R** and TYR altered the molecular conformation and stability of TYR, and further decreased the hydrophobicity of the amino acid residues in the vicinity of tyrosine residues to different extent. The thiosemicarbazido moiety of TSC-ISA-**R** played a crucial role in the inhibition, and the isatin moiety seemed to act as an auxiliary role for binding the hydrophobic protein pocket of the enzyme to facilitate the thiosemicarbazido moiety approaching the hydrophobic domain around active center. The substituent modifications of the C-5 of indoline ring could alter the characters of the resulting TSC-ISA-**R** in different degrees, which affected their affinity to TYR, *L*-DOPA-TYR complex as well as to *L*-DOPA, and therefore their inhibitory effects on TYR activity. DFT calculations were performed at B3LYP level with 6-31G (d) basis sets to further gain insight into the structural features of TSC-ISA-**R** molecules. The results indicated a different effect of –**R** on the electron distribution in HOMO of the inhibitor molecules. The frontier molecular orbital energy gap of TSC-ISA-**R** was shown to almost accord with the inhibition trend observed from the inhibitory assays.

Declaration of Competing Interest

The authors declare that they have no known competing financial interests or personal relationships that could have appeared to influence the work reported in this paper.

Acknowledgements

The authors greatly acknowledge the financial support to this study by the Hunan Innovation and entrepreneurship technology investment project under the grant no. 2018GK5002. The authors are grateful to Ms. Dandan Wang at the Analysis and Testing Center in Yancheng Institute of Technology for finishing the characterizations of all synthesized compounds.

Author contributions

J.W. Chen conceived the idea, completed the draft preparation, revision of the manuscript and supervised all researches. R. Cheng finished the synthesis of the inhibitors, as well as the inhibition measurements and result analysis. W.Y. Shi performed the theoretical calculations and data analysis. Q.Y. Yuan and Y.Q. Wang conducted all characterizations of the inhibitors, and other workers carried out the validation of the experimental results.

Appendix A. Supplementary material

Supplementary data to this article can be found online at https://doi.org/10.1016/j.saa.2021.119669.

References

[1] Y. Matoba, T. Kumagai, A. Yamamoto, H. Yoshitsu, M. Sugiyama, Crystallographic evidence that the dinuclear copper center of tyrosinase is flexible during catalysis, J. Biol. Chem. 281 (2006) 8981–8990.
[2] H. Decker, T. Schweikardt, F. Tuczek, The first crystal structure of tyrosinase: all questions answered?, Angew. Chem. Int. Edit. 45 (2006) 4546–4550.
[3] M. Sendovski, M. Kanteev, V.S. Ben-Yosef, N. Adir, A. Fishman, First structures of an active bacterial tyrosinase reveal copper plasticity, J. Mol. Biol. 405 (2011) 227–237.
[4] W.T. Ismaya, H.J. Rozeboom, A. Weijn, J.J. Mes, F. Fusetti, H.J. Wichers, B.W. Dijkstra, Crystal structure of agaricus bisporus mushroom tyrosinase: identity of the tetramer subunits and interaction with tropolone, Biochemistry 50 (2011) 5477–5486.
[5] N. Fujieda, S. Yabuta, T. Ikeda, T. Oyama, N. Muraki, G. Kurisu, S. Itoh, Crystal structures of copper-depleted and copper-bound fungal pro-tyrosinase: insights into endogenous cysteine-dependent copper incorporation, J. Biol. Chem. 288 (30) (2013) 22128–22140.
[6] A.Y. Chen, R.N. Adamek, B.L. Dick, C.V. Credille, C.N. Morrison, S.M. Cohen, Targeting metalloenzymes for therapeutic intervention, Chem. Rev. 119 (2) (2019) 1323–1455.
[7] H. Decker, R. Dillinger, F. Tuczek, How does tyrosinase work? Recent insights from model chemistry and structural biology, Angew. Chem. Int. Edit. 39 (9) (2000) 1591–1595.
[8] L.M. Mirica, M. Vance, D.J. Rudd, B. Hedman, K.O. Hodgson, E.I. Solomon, T.D. Stack, Tyrosinase reactivity in a model complex: an alternative hydroxylation mechanism, Science 308 (2005) 1890–1892.
[9] X. Lai, H.J. Wichers, M. Soler-Lopez, B.W. Dijkstra, Structure and function of human tyrosinase and tyrosinase-related froteins, Chem. Eur. J. 24 (2018) 47–55.
[10] N. Unver, P. Freyschmidt-Paul, S. Horster, H. Wenck, F. Stab, T. Blatt, H.P. Elsasser, Alterations in the epidermal-dermal melanin axis and factor XIIIa melanophages in senile lentigo and ageing skin, Brit. J. Dermatol. 155 (2006) 119–128.
[11] P. Thanigaimalai, M. Manickam, V. Namasivayam, Skin whitening agents: medicinal chemistry perspective of tyrosinase inhibitors, J. Enzym. Inhib. Med. Chem. 32 (2017) 403–425.

[12] P. Thanigaimalai, V. Namasivayam, M. Manickam, S.H. Jung, Inhibitors of melanogenesis: An updated review, J. Med. Chem. 61 (2018) 7395–7418.
[13] P. Thanigaimalai, M. Manickam, S.H. Jung, Recent development of signaling pathways inhibitors of melanogenesis, Cell. Signal. 40 (2017) 99–115.
[14] M. Sugumaran, Molecular mechanisms for mammalian melanogenesis Comparison with insect cuticular sclerotization1, FEBS Lett. 293 (1991) 4–10.
[15] H. Xu, X. Zhang, E. Karangwa, S. Xia, Correlating enzymatic browning inhibition and antioxidant ability of Maillard reaction products derived from different amino acids, J. Sci. Food Agr. 97 (2017) 4210–4218.
[16] V. Gray-Schopfer, C. Wellbrock, R. Marais, Melanoma biology and new targeted therapy, Nature 445 (2007) 851–857.
[17] Y.J. Kim, H. Uyama, Tyrosinase inhibitors from natural and synthetic sources: Structure, inhibition mechanism and perspective for the future, Cell Mol. Life Sci. 62 (2005) 1707–1723.
[18] E. Buitrago, A. Vuillamy, A. Boumendjel, W. Yi, G. Gellon, R. Hardre, C. Philouze, G. Serratrice, H. Jamet, M. Reglier, C. Belle, Exploring the interaction of N/S compounds with a dicopper center: tyrosinase inhibition and model studies, Inorg. Chem. 53 (2014) 12848–12858.
[19] S.Y. Lee, N. Baek, T.G. Nam, Natural, semisynthetic and synthetic tyrosinase inhibitors, J. Enzym. Inhib. Med. Chem. 31 (2016) 1–13.
[20] J. Chen, Q. Li, Y. Ye, Z. Huang, Z. Ruan, N. Jin, Phloretin as both a substrate and inhibitor of tyrosinase: Inhibitory activity and mechanism, Spectrochim. Acta A 226 (2020) 117642.
[21] S. Zolghadri, A. Bahrami, M.T. Hassan Khan, J. Munoz-Munoz, F. Garcia-Molina, F. Garcia-Canovas, A.A. Saboury, A comprehensive review on tyrosinase inhibitors, J. Enzym. Inhib. Med. Chem. 34 (2019) 279–309.
[22] K. Hałdys, R. Latajka, Thiosemicarbazones with tyrosinase inhibitory activity, Med. Chem. Commun. 10 (2019) 378–389.
[23] P. Cai, Y. Xiong, Y. Yao, W. Chen, X. Dong, Synthesis, screening and biological activity of potent thiosemicarbazone compounds as a tyrosinase inhibitor, New J. Chem. 43 (2019) 14102–14111.
[24] K. Hałdys, W. Goldeman, M. Jewgiński, E. Wolińska, N. Anger, J. Rossowska, R. Latajka, Inhibitory properties of aromatic thiosemicarbazones on mushroom tyrosinase: synthesis, kinetic studies, molecular docking and effectiveness in melanogenesis inhibition, Bioorg. Chem. 81 (2018) 577–586.
[25] T.S. Lobana, R. Sharma, G. Bawa, S. Khanna, Bonding and structure trends of thiosemicarbazone derivatives of metals—an overview, Coord. Chem. Rev. 253 (2009) 977–1055.
[26] S. Cao, X. Chen, L. Chen, J. Chen, α(N)-Heterocyclic thiosemicarbazones: Iron chelators that are promising for revival of gallium in cancer chemotherapy, Anti-Cancer Agents Med. Chem. 16 (2016) 973–991.
[27] M. Carcelli, D. Rogolino, J. Bartoli, N. Pala, C. Compari, N. Ronda, F. Bacciottini, M. Incerti, E. Fisicaro, Hydroxyphenyl thiosemicarbazones as inhibitors of mushroom tyrosinase and antibrowning agents, Food Chem. 303 (2020) 125310.
[28] K. Hałdys, W. Goldeman, M. Jewgiński, E. Wolińska, N. Anger-Góra, J. Rossowska, R. Latajka, Halogenated aromatic thiosemicarbazones as potent inhibitors of tyrosinase and melanogenesis, Bioorg. Chem. 94 (2020) 103419.
[29] P. Thanigaimalai, T.A. Hoang, K.C. Lee, S.C. Bang, V.K. Sharma, C.Y. Yun, E. Roh, B.Y. Hwang, Y. Kim, S.H. Jung, Structural requirement(s) of N-phenylthioureas and benzaldehyde thiosemicarbazones as inhibitors of melanogenesis in melanoma B 16 cells, Bioorg. Med. Chem. Lett. 20 (2010) 2991–2993.
[30] K.C. Lee, P. Thanigaimalai, V.K. Sharma, M.S. Kim, E. Roh, B.Y. Hwang, Y. Kim, S. H. Jung, Structural characteristics of thiosemicarbazones as inhibitors of melanogenesis, Bioorg. Med. Chem. Lett. 20 (2010) 6794–6796.
[31] P. Thanigaimalai, K.C. Lee, V.K. Sharma, E. Roh, Y. Kim, S.H. Jung, Ketonethiosemicarbazones: structure-activity relationships for their melanogenesis inhibition, Bioorg. Med. Chem. Lett. 21 (2011) 3527–3530.
[32] P. Thanigaimalai, E.V. Rao, K.C. Lee, V.K. Sharma, E. Roh, Y. Kim, S.H. Jung, Structure-activity relationship of naphthaldehydethiosemicarbazones in melanogenesis inhibition, Bioorg. Med. Chem. Lett. 22 (2012) 886–889.
[33] A. You, J. Zhou, S. Song, G. Zhu, H. Song, W. Yi, Rational design, synthesis and structure–activity relationships of 4-alkoxy- and 4-acyloxy-phenylethylenethiosemicarbazone analogues as novel tyrosinase inhibitors, Bioorg. Med. Chem. 23 (2015) 924–931.
[34] J. Xie, H. Dong, Y. Yu, S. Cao, Inhibitory effect of synthetic aromatic heterocycle thiosemicarbazone derivatives on mushroom tyrosinase: Insights from fluorescence, ^{1}HNMR titration and molecular docking studies, Food Chem. 190 (2016) 709–716.
[35] S. Song, A. You, Z. Chen, G. Zhu, H. Wen, H. Song, W. Yi, Study on the design, synthesis and structure-activity relationships of new thiosemicarbazone compounds as tyrosinase inhibitors, Eur. J. Med. Chem. 139 (2017) 815–825.
[36] M.A. Soares, M.A. Almeida, C. Marins-Goulart, O.A. Chaves, A. Echevarria, M.C. C. de Oliveira, Thiosemicarbazones as inhibitors of tyrosinase enzyme, Bioorg. Med. Chem. Lett. 27 (2017) 3546–3550.
[37] J. Liu, M. Li, Y. Yu, S. Cao, Novel inhibitors of tyrosinase produced by the 4-substitution of TCT (II), Intern. J. Biol. Macromol. 103 (2017) 1096–1106.
[38] D. Sousa-Pereira, O.A. Chaves, C.M. Dos Reis, M.C.C. de Oliveira, C.M.R. Sant'Anna, J.C. Netto-Ferreira, A. Echevarria, Synthesis and biological evaluation of N-aryl-2-phenyl-hydrazinecarbothioamides: experimental and theoretical analysis on tyrosinase inhibition and interaction with HSA, Bioorg. Chem. 81 (2018) 79–87.
[39] J.F.M.d. Silva, S.J. Garden, A.C. Pinto, The chemistry of isatins: a review from 1975 to 1999, J. Braz. Chem. Soc. 12 (2001) 273–324.
[40] A.M.S. El-Sharief, Y.A. Ammar, A. Belal, M. El-Sharief, Y.A. Mohamed, A.B.M. Mehany, G.A.M. Elhag Ali, A. Ragab, Design, synthesis, molecular docking and biological activity evaluation of some novel indole derivatives as potent anticancer active agents and apoptosis inducers, Bioorg. Chem. 85 (2019) 399–412.
[41] Varun, Sonam, R. Kakkar, Isatin and its derivatives: a survey of recent syntheses, reactions, and applications, Med. Chem. Commun. 10 (2019) 351–368.
[42] M.A. Ganim, M.C. Baloglu, A. Aygun, Y.C. Altunoglu, H.S. Sayiner, F. Kandemirli, F. Sen, Analysis of DNA protection, interaction and antimicrobial activity of isatin derivatives, Intern. J. Biol. Macromol. 122 (2019) 1271–1278.
[43] P. Mishra, A. Kumar, P. Mamidi, S. Kumar, I. Basantray, T. Saswat, I. Das, T.K. Nayak, S. Chattopadhyay, B.B. Subudhi, S. Chattopadhyay, Inhibition of *Chikungunya* virus replication by 1-[(2-methylbenzimidazol-1-yl)methyl]-2-oxo-indolin-3-ylidene]Amino] thiourea (MBZM-N-IBT), Sci. Rep. 6 (2016) 20122.
[44] J. Verbeek, J. Eriksson, S. Syvanen, M. Huisman, R.C. Schuit, C.F.M. Molthoff, R.A. Voskuyl, E.C. de Lange, A.A. Lammertsma, A.D. Windhorst, Synthesis and preliminary preclinical evaluation of fluorine-18 labelled isatin-4-(4-methoxyphenyl)-3-thiosemicarbazone ([^{18}F]$_4$FIMPTC) as a novel PET tracer of P-glycoprotein expression, EJNMMI Radiopharm. Chem. 3 (2018) 11.
[45] M. Muralisankar, R. Sreedharan, S. Sujith, N.S.P. Bhuvanesh, A. Sreekanth, N(1)-pentyl isatin-N(4)-methyl-N(4)-phenyl thiosemicarbazone (PITSc) as a corrosion inhibitor on mild steel in HCl, J. Alloy Compd. 695 (2017) 171–182.
[46] W.L.E. Armarego, D.D. Perrin, Purification of Laboratory Chemicals, fourth ed., Butterworth-Heinemann, Wodburn, MA, 2000.
[47] J.F. de Oliveira, A.L. da Silva, D.B. Vendramini-Costa, C.A. da Cruz Amorim, J.F. Campos, A.G. Ribeiro, R. Olimpio de Moura, J.L. Neves, A.L. Ruiz, J. Ernesto de Carvalho, C. Alves de Lima Mdo, Synthesis of thiophene-thiosemicarbazone derivatives and evaluation of their in vitro and in vivo antitumor activities, Eur. J. Med. Chem. 104 (2015) 148–156.
[48] M.D. Hall, K.R. Brimacombe, M.S. Varonka, K.M. Pluchino, J.K. Monda, J. Li, M.J. Walsh, M.B. Boxer, T.H. Warren, H.M. Fales, M.M. Gottesman, Synthesis and structure-activity evaluation of isatin-beta-thiosemicarbazones with improved selective activity toward multidrug-resistant cells expressing P-glycoprotein, J. Med. Chem. 54 (2011) 5878–5889.
[49] J. Liu, W. Yi, Y. Wan, L. Ma, H. Song, 1-(1-Arylethylidene)thiosemicarbazide derivatives: a new class of tyrosinase inhibitors, Bioorg. Med. Chem. 16 (2008) 1096–1102.
[50] R.A. Copeland, Evaluation of Enzyme Inhibitors in Drug Discovery, John Wiley & Sons, Inc. Publication, New Jersey, 2013.
[51] J. Yan, G. Zhang, J. Pan, Y. Wang, α-Glucosidase inhibition by luteolin: kinetics, interaction and molecular docking, Intern. J. Biol. Macromol. 64 (2014) 213–223.
[52] N. Shahabadi, M. Maghsudi, S. Rouhani, Study on the interaction of food colourant quinoline yellow with bovine serum albumin by spectroscopic techniques, Food Chem. 135 (2012) 1836–1841.
[53] M. Fan, G. Zhang, X. Hu, X. Xu, D. Gong, Quercetin as a tyrosinase inhibitor: Inhibitory activity, conformational change and mechanism, Food Res. Intern. 100 (2017) 226–233.
[54] M. Frisch, G. Trucks, H. Schlegel, G. Scuseria, M. Robb, J. Cheeseman, G. Scalmani, V. Barone, B. Mennucci, G. Petersson, 2009. Gaussian 09, Revision D. 01, Gaussian, Inc.: Wallingford, CT.
[55] S. Miertuš, E. Scrocco, J. Tomasi, Electrostatic interaction of a solute with a continuum. A direct utilization of *ab initio* molecular potentials for the prevision of solvent effects, Chem. Phys. 55 (1981) 117–129.
[56] T. Lu, F. Chen, Quantitative analysis of molecular surface based on improved marching tetrahedra algorithm, J. Mol. Graph. Model. 38 (2012) 314–323.
[57] J. Yoon, S. Fujii, E.I. Solomon, Geometric and electronic structure differences between the type 3 copper sites of the multicopper oxidases and hemocyanin/tyrosinase, Proc. Natl. Acad. Sci. USA 106 (2009) 6585–6590.
[58] J. Choi, S.J. Park, J.G. Jee, Analogues of ethionamide, a drug used for multidrug-resistant tuberculosis, exhibit potent inhibition of tyrosinase, Eur. J. Med. Chem. 106 (2015) 157–166.
[59] M.R. Links, J. Taylor, M.C. Kruger, J.R.N. Taylor, Sorghum condensed tannins encapsulated in kafirin microparticles as a nutraceutical for inhibition of amylases during digestion to attenuate hyperglycaemia, J. Funct. Foods 12 (2015) 55–63.
[60] M. Fan, H. Ding, G. Zhang, X. Hu, D. Gong, Relationships of dietary flavonoid structure with its tyrosinase inhibitory activity and affinity, LWT - Food Sci. Technol. 107 (2019) 25–34.
[61] D. Kim, J. Park, J. Kim, C. Han, J. Yoon, N. Kim, J. Seo, C. Lee, Flavonoids as mushroom tyrosinase inhibitors: a fluorescence quenching study, J. Agric. Food Chem. 54 (2006) 935–941.
[62] O.A. Chaves, M.C.C. de Oliveira, C.M.C. de Salles, F.M. Martins, B.A. Iglesias, D.F. Back, In vitro tyrosinase, acetylcholinesterase, and HSA evaluation of dioxidovanadium (V) complexes: An experimental and theoretical approach, J. Inorg. Biochem. 200 (2019) 110800.
[63] O.A. Chaves, T.P. Calheiro, J.C. Netto-Ferreira, M.C.C. de Oliveira, S.Z. Franceschini, C.M.C. de Salles, N. Zanatta, C.P. Frizzo, B.A. Iglesias, H.G. Bonacorso, Biological evaluation of BF_2-naphthyridine compounds: Tyrosinase and acetylcholinesterase activity, CT-DNA and HSA binding property evaluations, Intern. J. Biol. Macromol. 160 (2020) 1114–1129.
[64] O.A. Chaves, M.R. de Lima Santos, M.C.C. de Oliveira, C.M.R. Sant'Anna, R.C. Ferreira, A. Echevarria, J.C. Netto-Ferreira, Synthesis, tyrosinase inhibition and transportation behavior of novel β-enamino thiosemicarbazide derivatives by human serum albumin, J. Mol. Liq. 254 (2018) 280–290.

[65] P.N. Naik, S.A. Chimatadar, S.T. Nandibewoor, Interaction between a potent corticosteroid drug–dexamethasone with bovine serum albumin and human serum albumin: a fluorescence quenching and fourier transformation infrared spectroscopy study, J. Photochem. Photobiol. B: Biology 100 (2010) 147–159.
[66] H. Baltacioglu, A. Bayindirli, M. Severcan, F. Severcan, Effect of thermal treatment on secondary structure and conformational change of mushroom polyphenol oxidase (PPO) as food quality related enzyme: a FTIR study, Food Chem. 187 (2015) 263–269.
[67] M. Tse, S. Kermasha, A. Ismail, Biocatalysis by tyrosinase in organic solvent media: A model system using catechin and vanillin as substrates, J. Mol. Catal. B: Enzym. 2 (1997) 199–213.
[68] K. Cai, X. Zheng, Y. Liu, S. Liu, F. Du, Correlation between amide-I spectra and structural features of glycine dipeptide, Acta Phys.-Chim. Sin. 32 (5) (2016) 1289–1296.
[69] M. Fan, G. Zhang, J. Pan, D. Gong, An inhibition mechanism of dihydromyricetin on tyrosinase and the joint effects of vitamins B6, D3 or E, Food Funct. 8 (2017) 2601–2610.
[70] S. Khatib, O. Nerya, R. Musa, S. Tamir, T. Peter, J. Vaya, Enhanced substituted resorcinol hydrophobicity augments tyrosinase inhibition potency, J. Med. Chem. 50 (2007) 2676–2681.
[71] S. Beheshti, A. Shayanfar, Prediction of the oral bioavailability correlation between humans and preclinical animals, Eur. J. Drug Metab. Pharmacokinet. (2020).
[72] C. Hansch, A. Leo, R.W. Taft, A survey of Hammett substituent constants and resonance and field parameters, Chem. Rev. 91 (1991) 165–195.
[73] W. Yi, C. Dubois, S. Yahiaoui, R. Haudecoeur, C. Belle, H. Song, R. Hardré, M. Réglier, A. Boumendjel, Refinement of arylthiosemicarbazone pharmacophore in inhibition of mushroom tyrosinase, Eur. J. Med. Chem. 46 (2011) 4330–4335.
[74] A. Yoshimori, T. Oyama, S. Takahashi, H. Abe, T. Kamiya, T. Abe, S. Tanuma, Structure-activity relationships of the thujaplicins for inhibition of human tyrosinase, Bioorg. Med. Chem. 22 (2014) 6193–6200.
[75] L. Kubik, W. Struck-Lewicka, R. Kaliszan, P. Wiczling, Simultaneous determination of hydrophobicity and dissociation constant for a large set of compounds by gradient reverse phase high performance liquid chromatography-mass spectrometry technique, J. Chromatogr. A 1416 (2015) 31–37.
[76] C.G. Swain, E.C. Lupton, Field and resonance components of substituent effects, J. Am. Chem. Soc. 90 (1968) 4328–4337.
[77] M. Charton, Electrical effect substituent constants for correlation analysis, in: R.W. Taft (Ed.), Prog. Phys. Org. Chem., vol. 13, John Wiley & Sons, Inc., 2007.
[78] M. Saranya, S. Ayyappan, R. Nithya, R.K. Sangeetha, A. Gokila, Molecular structure, NBO and HOMO-LUMO analysis of quercetin on single layer grapheme by density functional theory, Digest J. Nanomater. Biostruct. 13 (2018) 97–105.
[79] M.T. Hassan Khan, Molecular design of tyrosinase inhibitors: a critical review of promising novel inhibitors from synthetic origins, Pure Appl. Chem. 79 (2007) 2277–2295.
[80] S. Sudha, N. Sundaraganesan, M. Kurt, M. Cinar, M. Karabacak, FT-IR and FT-Raman spectra, vibrational assignments, NBO analysis and DFT calculations of 2-amino-4-chlorobenzonitrile, J. Mol. Struct. 985 (2011) 148–156.
[81] S.B. Gopalakrishnan, T. Kalaiarasi, R. Subramanian, Comparative DFT study of phytochemical constituents of the fruits of Cucumis trigonus Roxb. and Cucumis sativus Linn., J. Comput. Method Phys. 2014 (2014) 1–6.
[82] G. Kirishnamaline, J.D. Magdaline, T. Chithambarathanu, D. Aruldhas, A.R. Anuf, Theoretical investigation of structure, anticancer activity and molecular docking of thiourea derivatives, J. Mol. Struct. 1225 (2021) 129118.